

CONFIDENTIAL

Copy
RM L52L05

NACA RM L52L05



MAR 19 1953



RESEARCH MEMORANDUM

WIND-TUNNEL INVESTIGATION OF STALL
CONTROL BY SUCTION THROUGH A POROUS LEADING EDGE ON
A 37° SWEEPBACK WING OF ASPECT RATIO 6 AT REYNOLDS
NUMBERS FROM 2.50×10^6 TO 8.10×10^6

By Robert R. Graham and William A. Jacques

Langley Aeronautical Laboratory
Langley Field, Va.

CLASSIFICATION CANCELLED

Authority Doc R-7-3013 Date 6/10/53

By MTA 6/22/53 See _____

CLASSIFIED DOCUMENT

This material contains information affecting the National Defense of the United States within the meaning of the espionage laws, Title 18, U.S.C., Secs. 793 and 794, the transmission or revelation of which in any manner to an unauthorized person is prohibited by law.

NATIONAL ADVISORY COMMITTEE FOR AERONAUTICS

WASHINGTON
March 11, 1953

~~CONFIDENTIAL~~ NACA LIBRARY
LANGLEY AERONAUTICAL LABORATORY
Langley Field, Va.

NATIONAL ADVISORY COMMITTEE FOR AERONAUTICS

RESEARCH MEMORANDUM

WIND-TUNNEL INVESTIGATION OF STALL
CONTROL BY SUCTION THROUGH A POROUS LEADING EDGE ON
A 37° SWEEPBACK WING OF ASPECT RATIO 6 AT REYNOLDS
NUMBERS FROM 2.50×10^6 TO 8.10×10^6

By Robert R. Graham and William A. Jacques

SUMMARY

The effects of suction through a porous leading-edge surface have been investigated in the Langley 19-foot pressure tunnel on a wing having 37° sweepback of the leading edge, an aspect ratio of 6, taper ratio of 0.5, and NACA 64₁-212 airfoil sections normal to the 27-percent-chord line. The effects of varying the chordwise and spanwise extent of porous area were investigated on the wing without trailing-edge flaps and the effects of one chordwise and spanwise extent of porous area were investigated on the wing with half-span split and double slotted flaps. The tests covered a range of Reynolds number from 2.50×10^6 to 8.10×10^6 and a range of Mach number from 0.08 to 0.26.

The results indicate that at Mach numbers of the order of 0.12 the outboard stall of the wing can be delayed and nose-down moments at maximum lift can be produced about as effectively by boundary-layer control as by a leading-edge flap or slat. Suction over the outer 50 percent of the semispan controlled the tip stall and allowed maximum lift coefficients of 1.33, 1.49, and 1.90 to be attained with trailing-edge flaps neutral, half-span split flap deflected, and half-span double slotted flap deflected, respectively. When a leading-edge flap was deflected on the same portion of the solid-leading-edge wing, corresponding values of 1.39, 1.46, and 1.87 were attained.

At a free-stream Mach number of 0.26, the wing with leading edge sealed stalled when sonic velocity was reached locally. The limited suction available, at that Mach number, delayed the tip stall until a local Mach number of 1.20 was reached but did not provide nose-down moments.

~~SECRET~~

INTRODUCTION

Considerable research in recent years has been carried on for the purpose of improving the low-speed longitudinal stability of sweptback wings. Most of this work has been concerned with delaying the tip stall by means of auxiliary devices such as leading-edge flaps, slats, or droop nose. (See, for instance, refs. 1 to 3.) More recently, attention has been directed toward the possibility that stability at the stall might be obtained just as effectively by means of boundary-layer control.

Some data are available which demonstrate that longitudinal stability at the stall can be improved on sweptback wings by means of suction through leading-edge slots or porous area (refs. 4 to 6). An appraisal of leading-edge suction as a stall-control device on sweptback wings, however, can be made only if its effects can be directly compared with the effects of auxiliary devices on the same wing. In order to make this comparison and also to provide additional data showing the effects of leading-edge suction on sweptback wings, an investigation was made in the Langley 19-foot pressure tunnel on a 37° sweptback wing of aspect ratio 6 with suction through a porous leading edge. The effects of auxiliary devices on the same wing are shown in reference 1.

The tests included a few made with half-span split or double slotted flaps deflected and were made over a range of Reynolds number from 2.50×10^6 to 8.10×10^6 and a range of Mach number from 0.08 to 0.26.

SYMBOLS

Forces and moments on the wing are referred to the wind axes with the origin at the quarter-chord point of the mean aerodynamic chord. All coefficients and dimension symbols refer to the model as a complete wing.

C_L	lift coefficient, $Lift/q_0S$
$C_{L_{max}}$	maximum lift coefficient
C_D	drag coefficient, $Drag/q_0S$
C_{Dp}	equivalent pump-power drag coefficient, $C_p C_Q$
C_m	pitching-moment coefficient, $\frac{\text{Pitching moment about } 0.25\bar{c}}{q_0 S \bar{c}}$

~~SECRET~~

C_p	suction-duct pressure coefficient, $\frac{H_d - H_o}{q_o}$
C_Q	suction-flow coefficient, $Q/V_o S$
P	pressure coefficient, $\frac{p - p_o}{q_o}$
P_{Cr}	pressure coefficient for local sonic velocity
R	Reynolds number, $\rho_o V_o \bar{c} / \mu$
M	free-stream Mach number, V_o / a
M_λ	local Mach number, $\sqrt{\frac{5 + M^2 \cos^2 \Lambda}{(0.7 M^2 + 1)^{1/3.5}}} - 5$
α	angle of attack of root chord, deg
H_d	duct total pressure inside porous leading edge
Q	volume flow, at free-stream density, through porous surface
p	local static pressure
S	total wing area
S'	wing area affected by suction (See table I)
b	wing span
\bar{c}	mean aerodynamic chord, $\frac{2}{S} \int_0^{b/2} c^2 dy$
c	local wing chord parallel to plane of symmetry
y	lateral coordinate
Λ	sweep of leading edge
q_o	free-stream dynamic pressure, $\frac{1}{2} \rho_o V_o^2$

p_o	free-stream static pressure
H_o	free-stream total pressure
V_o	free-stream velocity
ρ_o	free-stream air density
μ	coefficient of viscosity
a	speed of sound

MODEL AND APPARATUS

The model used in this investigation was a semispan wing mounted in the presence of a reflection plane as shown in figure 1. A photograph of the model and reflection plane mounted in the tunnel is presented as figure 2. Except for the modified leading edge, the wing was the same one described in reference 1. It had an aspect ratio of 6, a taper ratio of 0.5, and 37.25° sweepback of the leading edge. The airfoil sections were of NACA 64₁-212 profile perpendicular to the 27-percent-chord line. The general plan form and some of the principal dimensions of the model are given in figure 3.

For several tests the model was fitted with 0.50b/2 split flaps, 0.50b/2 double slotted flaps, and a fence at the 0.50b/2 station, details of which are presented in figure 4.

The leading edge of the upper surface was constructed from a laminated skin attached to solid ribs. Two skins were tested, both of which consisted of 1/16-inch perforated plate covered with a layer of 14 x 18 mesh bronze screen and an outer surface of 30 x 250 mesh, Dutch weave, Monel filter cloth. The filter cloth was rolled from its original thickness of 0.026 inch to 0.018 inch for one of the skins and to 0.016 inch for the other skin to obtain the desired values of porosities and a smooth surface of the skin. The porosity characteristics of the two skins as installed on the model are shown in figure 5. The porosity of the skin with 0.018-inch filter cloth is designated as porosity A and that for the skin with 0.016-inch filter cloth is designated as porosity B. A third porosity was inadvertently tested in the beginning of the test program when the porosity of the 0.016-inch filter cloth was reduced by the corrosive action of soldering flux which had been used only along the edge of the skin in the fabrication process but which apparently penetrated the entire area of the skin by capillary action. This porosity is designated as porosity C and was used for only a few tests before the skin

was cleaned by means of hydrochloric acid, water, and steam to increase the porosity to that designated as porosity B. The 0.018-inch filter cloth was cemented in place; hence, no corrosion problem occurred.

The solid ribs which supported the porous skin divided the leading edge into eight compartments the dimensions of which are shown in figure 2. Each compartment was connected to the main suction duct through an individual flow-measuring venturi and flow-control gate valve.

Flow into the leading edge of the wing was obtained by connecting the suction duct to the outside of the tunnel when the air in the tunnel was compressed to about $2\frac{1}{3}$ atmospheres or to high-capacity vacuum pumps when the air in the tunnel was at atmospheric pressure.

The extent of the porous area was controlled by spraying the leading edge with a layer of nonporous strippable plastic and a layer of lacquer sanded smooth and then stripping off only the area which was to be porous. The porosity of the skin was maintained by passing a cleaning agent such as acetone or carbon tetrachloride through the porous area.

The leading edge of the wing was equipped with surface orifices at 0, 0.001c, 0.003c, and 0.005c at the spanwise midpoint of each compartment to measure the peak leading-edge pressures at those spanwise locations. Each compartment was equipped with a tube for measuring the total pressure inside the leading edge.

Tests

The tests were made in the Langley 19-foot pressure tunnel. The majority of the tests were made with the air in the tunnel compressed to about $2\frac{1}{3}$ atmospheres. The Reynolds number range for those tests was

4.36×10^6 to 8.10×10^6 and the corresponding Mach number range was 0.08 to 0.15. In order to investigate some of the effects of compressibility, a few tests were made with the air in the tunnel at atmospheric pressure. The Mach number range for those tests was 0.10 to 0.26 and the corresponding Reynolds number range was 2.50×10^6 to 6.30×10^6 .

Lift, drag, and pitching-moment data were obtained through an angle-of-attack range extending beyond maximum lift. Airfoil peak pressures and suction-flow rates were also obtained through this range. The extent of porous area was varied spanwise between the 0.15b/2 station and the 0.95b/2 station and chordwise between 0 and 0.10c on the upper surface.

Tests were made to investigate the effects of suction on the plain wing, the wing with 0.50b/2 split flaps, and the wing with 0.50b/2 double

slotted flaps. An upper-surface fence at the $0.50b/2$ station was also tested on the preceding configurations.

A few tests were made with the porous skin exposed but with the suction valve closed to simulate suction-power failure.

All the tests with suction were made with the pressure inside the leading edge constant along the span. The pressure was varied through the angle-of-attack range, however, in order to maintain a constant value of flow coefficient C_Q .

CORRECTIONS TO DATA

The lift, drag, and pitching-moment data presented herein have been corrected for air-stream misalignment but have not been corrected for support tare and interference effects. Previous experience on complete models indicates that corrections for the effects of the tare and interference caused by the model supports consist of (1) a constant shift in the pitching-moment curve (about -0.008), (2) a slight increase in lift-curve slope (about 0.0008), and (3) a decrease in drag in the low lift range.

Jet-boundary corrections obtained by combining the methods of references 7 and 8 were made to the angle of attack and to the drag coefficient and are as follows:

$$\Delta\alpha = 1.12C_L$$

$$\Delta C_D = 0.0164C_L^2$$

The correction to the pitching-moment coefficient caused by the tunnel-induced distortion of the loading is

$$\Delta C_m = 0.0101C_L$$

An additional drag correction was required in these tests because the air drawn into the wing was discharged at right angles to the air stream, thus creating a drag force equal to that caused by loss of momentum of the suction air in the drag direction. The assumption was made that the momentum of the suction air was that in the free stream and that

no losses occurred in the wing boundary layer prior to entering the wing. The drag correction determined from impulse momentum principles is

$$\Delta C_{DQ} = -2C_Q$$

RESULTS AND DISCUSSION

The results of the investigation are summarized in table II. Detailed results from some of the more interesting configurations are presented in figures 6 to 33.

Wing Without Flaps

Wing characteristics with leading edge sealed.- A comparison of the lift and pitching-moment characteristics as shown in figure 6 with those of reference 1 indicates that at Reynolds numbers above 4.36×10^6 the installation of the sealed porous skin caused the initial separation and final stall to occur at lower lift coefficients and lower angles of attack than those for the wing with the solid leading edge. At the lower Reynolds numbers (2.50×10^6 to 3.50×10^6) the installation of the sealed porous skin had practically no effect. The maximum lift coefficient for the wing at a Reynolds number of 6.80×10^6 was 1.15 with the leading edge sealed and sanded smooth, as compared with 1.27 with the solid steel leading edge. A similar reduction in maximum lift was noted in reference 1 when the wing was tested with a slat in the retracted position ($C_{L_{max}} = 1.17$). These differences in maximum lift indicate the effects of small changes in the leading-edge contour on the wing stall and demonstrate the difficulty of accurately fabricating a smooth leading edge as compared with accurately machining one from solid material.

Figure 6 also shows the effects of varying the Reynolds numbers through a range from 2.50×10^6 to 8.10×10^6 at Mach numbers below 0.15. The value of $C_{L_{max}}$ varied from 1.04 at 2.50×10^6 to 1.15 at 6.80×10^6 and 1.13 at 8.10×10^6 . The lift coefficient at which the unstable pitching-moment break occurred changed from about 0.9 at $R = 2.50 \times 10^6$ to about 1.1 at the higher Reynolds numbers, thus indicating that the initial trailing-edge separation was delayed to a higher angle of attack.

The plots of peak measured pressure coefficient across the span of the wing (fig. 7) show the progression of the leading-edge stall as the angle of attack is increased in the range near $C_{L_{max}}$. At the lowest Reynolds number of the tests (2.50×10^6) the stall originated in the tip area and spread inboard as the angle of attack was increased. As the Reynolds number was increased to 4.36×10^6 the initial stall was delayed to a higher angle of attack, but it covered a larger outboard area than at the lower Reynolds numbers. Further increases in Reynolds number caused a reduction in area of the initial stall and a more gradual spread of the stall with increasing angle of attack.

The effects of varying the Reynolds number combined with those due to compressibility are shown in figure 8 where the Reynolds number was varied from 2.50×10^6 to 6.37×10^6 as the Mach number was varied from 0.10 to 0.26. The value of $C_{L_{max}}$ increased from 1.03 to 1.13 as the Mach number was increased from 0.10 to 0.20 but decreased to 1.09 as the Mach number was further increased to 0.26. The increase in $C_{L_{max}}$ as the Mach number was increased from 0.10 to 0.20 was, of course, due to the corresponding increase in Reynolds number from 2.50×10^6 to 4.95×10^6 . The decrease in $C_{L_{max}}$ that occurred as the Mach number was increased above 0.20 was due to compressibility effects. Figure 9 shows that the peak measured leading-edge pressure coefficient for the plain wing reached a value of -11.2 at a Mach number of 0.20 and decreased as the Mach number was increased. At a Mach number of 0.26 the peak measured leading-edge pressure indicated that sonic velocity had been reached locally. At that Mach number the local attainment of sonic velocity apparently precipitated the stall. At Mach numbers between 0.20 and 0.26 the data do not indicate that sonic velocity was attained, but it may possibly have been attained at some location and angle of attack between those at which measurements were taken.

The plots of peak measured pressure coefficient across the span of the wing (fig. 10) show that the angle of attack at which the outboard stall occurred did not change through the Mach number range from 0.14 to 0.24. Apparently increasing the Mach number above 0.14 offsets the effects of the corresponding increase in Reynolds number above 3.46×10^6 . Comparison of figures 7 and 10 shows that at a Reynolds number of about 4.40×10^6 the outboard stall occurs at an angle of attack of 17.30° at a Mach number of 0.08 and 15.20° at 0.18. A corresponding reduction in the angle of attack for the outboard stall was brought about at a Reynolds number of about 5.40×10^6 when the Mach number was increased from 0.10 to 0.22 and at about 6.50×10^6 when the Mach number was increased from 0.12 to 0.26.

Effects of varying spanwise extent of porous skin.- The data of figures 11 and 12 reveal that suction through the outboard 50 percent ($0.45b/2$ to $0.95b/2$) of the leading edge of the wing at a Reynolds number of 6.80×10^6 increased the maximum lift coefficient $C_{L_{max}}$ from 1.15 to as much as 1.35 depending on the chordwise extent of porous area, the porosity, and the flow coefficient. Extending the porous area inboard as far as the $0.15b/2$ station resulted in a slight decrease in $C_{L_{max}}$ for the flow rates obtained. If it had been possible to obtain higher flow rates, higher values of $C_{L_{max}}$ might have been obtained. Suction over less than the outer 50 percent of the semispan resulted in no increase in $C_{L_{max}}$ over the values for the sealed-leading-edge configuration.

The data of figures 11 and 12 show that leading-edge suction was required only on the outer 37 percent to 50 percent of the semispan to alleviate the sharp unstable pitching moments in the high lift range. Suction at the maximum flow rates available over less than the outer 37 percent or over more than the outer 50 percent of the semispan caused the pitching moments to be stable at $C_{L_{max}}$ but did not prevent a serious unstable trend from occurring just below $C_{L_{max}}$.

The plots of leading-edge peak pressures across the span (fig. 13) show that suction over the outer 25 percent of the semispan at the rates obtained did not delay the stall in that area but did maintain some lift over that portion of the wing as the stall progressed inboard. Thus the initial outboard stall caused nose-up moments but enough lift was maintained over that portion of the wing so that as the stall progressed inboard the moments changed to a nose-down direction. Extending the porous area inboard until it included the outer 50 percent of the semispan caused the stall to be delayed to a higher angle of attack but the suction was not sufficient to prevent a stall from occurring near the tip at the same time that a stall occurred just inboard of the porous area. The lift that was maintained on the outer portion of the wing, however, was sufficient to cause the pitching moment at the stall to be in a nose-down direction. The area between the two stalled areas maintained a fairly large peak pressure and consequently a fairly large lift to the highest angle of attack tested. When the porous area was extended well inboard, a fairly large part of the outer semispan stalled when the inboard sections stalled and the portion which maintained lift was too far inboard to contribute much to the pitching moments. Thus the data indicate that, if nose-down moments are to be obtained at the stall, the spanwise extent of porosity should be limited to about the outer 50 percent of the semispan. It is possible that nose-down moments could be obtained at the stall with a longer spanwise extent of porosity if the flow coefficient could be increased over the outboard sections.

Effects of varying chordwise extent of porous skin.- Figure 14 shows the effects of varying the chordwise extent of the porous area while holding the spanwise extent constant (outboard 50 percent of the semispan). The flow rates used were those obtained with the maximum pressure drop available so that the duct pressure coefficient was unchanged regardless of extent of porous area. Thus the pressure drop across the skin and the local flow rates through the porous skin at any particular angle of attack remained unchanged as the chordwise extent of porosity was varied. The total flow rate, however, increased as the extent of porous area was increased. The data (fig. 14) show that suction over only the leading 0.0055c of the upper surface of the outer 50 percent of the semispan was sufficient to delay the leading-edge stall so that nose-down pitching moments were obtained at $C_{L_{max}}$. The outboard trailing-edge separation, however, still occurred just below $C_{L_{max}}$ as evidenced by the unstable pitching-moment trend in that lift range. Increasing the chordwise extent of porous area caused a slight increase in $C_{L_{max}}$ and also reduced the range of instability prior to $C_{L_{max}}$.

The plots of leading-edge pressure (fig. 15) show that suction through the leading 0.0055c of the outer 50 percent of the semispan delayed the outboard stall from $\alpha = 16.4^\circ$ to $\alpha = 18.4^\circ$, but the inboard stall did not occur until 19.4° , with the result that nose-up moments were obtained when the outboard stall occurred. Suction from 0.001c to 0.010c on the same portion of the span delayed the outboard stall until an inboard stall had developed and maintained the high leading-edge peak pressures almost at the maximum obtained as the inboard stall developed. Increasing the chordwise extent delayed the tip stall to higher angles of attack and allowed higher pressure coefficients to be reached over the suction portion of the wing after the inboard portion was stalled.

Effects of varying suction flow rate.- The data of figure 16 show that, at a Reynolds number of 6.80×10^6 , reducing the flow rate from the maximum obtained with 0.015c chordwise extent and 50-percent spanwise extent of suction reduced the maximum lift coefficient from 1.33 for a C_Q of 0.00052 to 1.19 for a C_Q of 0.00018. The pitching moments were stable at the stall for values of C_Q of 0.00026 or greater but the unstable trend below $C_{L_{max}}$ was more severe at the lower flow rates. Tests at higher flow rates and reduced Reynolds numbers indicate that increasing the flow coefficient did not completely eliminate the unstable trend prior to $C_{L_{max}}$. Thus the tests indicate that leading-edge suction delayed leading-edge separation, with the result that considerable improvement in stability was obtained at $C_{L_{max}}$. They also indicate that leading-edge suction did not eliminate trailing-edge separation but did delay its

spread toward the leading edge, with the result that the unstable trend below $C_{L_{max}}$ was less severe with suction. It is possible that a mid-chord suction slot or suction area operating in conjunction with leading-edge suction (similar to the two-dimensional arrangement in ref. 9) might delay the trailing-edge separation so that the pitching-moment curve would be linear up to $C_{L_{max}}$.

The effects of varying suction rates on the leading-edge pressures are shown in figure 17. The minimum flow coefficient tested ($C_Q = 0.00018$) delayed the outboard leading-edge stall slightly, as shown by a comparison of the data of figure 17 with the data of figure 7 obtained at the same Reynolds number with leading edge sealed. An increase in $C_{L_{max}}$ was obtained with the minimum flow coefficient (see fig. 16), but that amount of suction did not maintain enough lift over the outboard portion of the wing to cause any improvement in the pitching-moment characteristics. Increasing the suction rate to a C_Q of 0.00040 delayed the stall to a higher angle of attack ($\alpha = 19.5^\circ$) and caused an increase in the outboard lift beyond the stall which considerably improved the pitching-moment characteristics at $C_{L_{max}}$. The lift that was maintained over the outboard sections after the stall occurred was sufficient to cause the pitching moments to be in a nose-down direction. A further increase in C_Q to the maximum that could be obtained at that Reynolds number ($C_Q = 0.00052$) did not cause any appreciable change in the spanwise distribution of the peak pressure coefficients or in the pitching-moment characteristics. Some data were obtained with a C_Q of 0.00090 but the Reynolds number was reduced to 4.36×10^6 and the effects of the Reynolds number reduction on the inboard stall tend to cloud any effects of the increased flow rate.

Scale effects with suction.- The effects of varying the Reynolds number of tests of the wing with suction from 0 to 0.015c and 0.45b/2 to 0.95b/2 are shown in figures 18 and 19. Figure 18 shows that with a constant flow coefficient ($C_Q = 0.00040$) the lift coefficient at which a severe nose-down change occurred in the pitching-moment curve was about constant at 1.26 through the Reynolds number range from 4.36×10^6 to 8.10×10^6 . Below a C_L of 1.26 the pitching-moment characteristics were similar throughout that Reynolds number range. One test was made at a Reynolds number of 3.46×10^6 and a C_Q of 0.00036. Under these conditions the pitching-moment characteristics were similar to those obtained at higher Reynolds numbers with $C_Q = 0.00040$ except that the severe change in the pitching-moment curve occurred at a lower lift coefficient (1.21).

Reference 6 indicates that with varying Reynolds number, dynamic similarity in the boundary layer will not be obtained with suction unless the product $C_Q R^{1/2}$ is held constant. Figure 19 shows that the pitching-moment characteristics and the values of $C_{L_{max}}$ were essentially the same through the Reynolds number range from 4.36×10^6 to 8.10×10^6 when $C_Q R^{1/2}$ was held constant or when C_Q alone was held constant (see fig. 18). Small differences in the pitching-moment characteristics are probably due to scale effects on the stalling characteristics of the sections inboard of the porous part of the leading edge.

The spanwise plots of leading-edge pressure coefficients (figs. 20 and 21) show only slight variations in distribution over the outboard portion of the wing with suction as the Reynolds number was varied whether the product $C_Q R^{1/2}$ was held constant at approximately $0.00040 \sqrt{8.10 \times 10^6}$ or C_Q was held constant at approximately 0.00040. In either case, however, when the stall occurred it covered a larger inboard (no suction) portion of the wing at the low Reynolds number than at the high Reynolds numbers.

Effects of leading-edge suction on wing characteristics at critical speeds.- Some of the effects of suction on the wing were determined at speeds at which critical or supercritical pressure coefficients were measured at the leading edge of the model. The results are not conclusive because only small flow coefficients were obtainable at those velocities. The results (figs. 8 and 22) indicate, however, that the small flow rate used at $M = 0.26$ ($C_Q \approx 0.00015$) was sufficient to delay the tip stall somewhat although not enough to cause nose-down pitching moments at $C_{L_{max}}$. The nose-up moment due to tip stall occurred at a lift coefficient about 0.04 greater than the corresponding lift coefficient with leading edge sealed. In order to accomplish this delay in the tip stall, the suction was required to maintain the flow around the leading edge even though that flow reached slightly supersonic local velocities ($M_l = 1.20$). Figure 9 shows the increase in the outboard leading-edge pressure coefficient (-9.3 to -12.2) brought about by suction through the porous skin ($C_Q \approx 0.00015$).

The spanwise plots of leading-edge pressure coefficient (figs. 10 and 23) show that at a Mach number of 0.26 a flow coefficient of about 0.00015 increases the angle of attack for the outboard stall from 14.2° to 15.3° and maintains some lift over that portion of the wing after the stall. The flow coefficient was not sufficient, however, to delay the outboard stall until an inboard stall had developed. The results show similar changes at lower Mach numbers except that a much larger increase in angle of attack for stall was brought about by $C_Q \approx 0.00015$ at the

lowest Mach number and Reynolds number than at the higher Mach numbers. At a Reynolds number of 2.50×10^6 and a Mach number of 0.10, the stall originated on the inboard portion of the wing and lift was maintained on the outer portion well beyond the stall so that the pitching moments were in a nose-down direction. When the flow was increased to the maximum obtainable at the lower Mach numbers, the pitching-moment characteristics were improved (table II) and the leading-edge pressure coefficients (fig. 24) indicated a larger lift maintained over the outer portion after the inboard stall had occurred.

Effects of leading-edge suction on the wing drag.- The effects of various rates of suction on the drag of the wing are shown in figure 25. It can be seen that suction has no effect on the drag except in the range of lift coefficient where the suction has delayed separation. The drag data indicate that, in the case of power failure, separation occurs at a much lower lift coefficient than with the leading edge sealed and the drag coefficient increases rapidly at lift coefficients above 0.8. Comparison of the drag data with those from reference 1 with a leading-edge flap on the same portion of the model as was occupied by the porous area ($0.45b/2$ to $0.95b/2$) shows that, as would be expected, the wing drag was less with suction than with the leading-edge flap. When the equivalent pump-power drag coefficient C_{DP} for C_Q greater than 0.00030 is added to the wing drag, however, the total drag is greater than the drag of the wing with leading-edge flap.

Effects of upper-surface fences.- Figure 26 shows that a fence on the upper surface of the wing at $0.50b/2$ delayed the trailing-edge separation so that the unstable pitching-moment trend below C_{Lmax} was considerably improved and in some cases was almost eliminated. The fence, however, had no effect on the leading-edge separation so that about the same suction flow was required to produce nose-down moments at the stall with or without the fence. (See table II.)

No attempt was made to determine the optimum fence arrangement but the trends indicated by the tests with one fence are similar to the trends shown in reference 10, which reports a more complete fence investigation.

The spanwise plots of peak pressure coefficient (figs. 17 and 27) show that, with suction, the angle of attack at which the initial stall occurred was about 1° lower for the configuration with fence than for the plain-wing configuration. When the leading edge was porous but no suction was applied, the fence had no noticeable effect on the stall as analyzed from the leading-edge pressures.

Wing With Trailing-Edge Flaps

The effects of leading-edge suction on the wing with trailing-edge flaps are shown in figures 28 to 30. Comparison of the data of figure 28 with corresponding data from reference 1 shows that, with half-span split flaps, the installation of the sealed porous skin on the model caused a reduction of $C_{L_{max}}$ to 1.36 from 1.55 for the solid leading edge. Applying suction to the leading 0.015c of the upper surface on the outer 50 percent of the semispan at a flow coefficient of 0.00048 increased $C_{L_{max}}$ to 1.49.

The wing exhibited nose-up pitching moments at the stall with the leading edge sealed, just as it did with the solid leading edge. With suction the pitching moments were in a nose-down direction at the stall, but just below $C_{L_{max}}$ they showed a nose-up trend similar to that noted when the flaps were neutral.

A comparison of the data for the wing with suction (fig. 28) with that for the wing with a leading-edge flap on the same portion of the wing (ref. 1) shows that the maximum lift coefficient was about the same for both configurations (1.49 and 1.46). The wing with leading-edge flap, however, exhibited practically linear pitching-moment characteristics below the stall as well as nose-down moments at the stall. One test was made with a fence at 0.50b/2 but the results (fig. 28) showed no effect on the pitching-moment characteristics and a slight reduction in $C_{L_{max}}$ (1.49 to 1.45).

The results of tests with the half-span double slotted flap (fig. 29) show that suction through the leading 0.015c of the upper surface on the outer 50 percent of the semispan at a C_Q of 0.00048 was slightly better than the leading-edge flap (ref. 1) on the same portion of the wing in terms of $C_{L_{max}}$ (1.90 compared with 1.87) and stability at the stall.

Both configurations, however, produced a loop in the pitching-moment curve at the stall such that nose-up moments were obtained at $C_{L_{max}}$ but nose-down moments as the lift dropped off in the stall. The fence at 0.50b/2 on the wing with suction failed to change the loop in the pitching-moment curve appreciably and caused a slight reduction in $C_{L_{max}}$ (1.90 to 1.85).

The effects of suction on the characteristics of the wing with double slotted flaps were also investigated at a Mach number where the stall was precipitated by compressibility effects ($M = 0.24$). The results (fig. 30) are inconclusive, however, because the maximum C_Q obtainable was only 0.00016. The value of $C_{L_{max}}$ was increased from 1.68 to 1.72 by that flow but the pitching-moment characteristics were unaffected (nose-up at the stall).

The effects of suction on the leading-edge pressures of the wing with flaps are shown in figure 31. The leading-edge pressures indicate that the initial stall and stall progression with flaps are similar to those without flaps. The stall with double slotted flaps is so much like that without flaps that no indication is given of the reason for the loop in the pitching-moment curve. Figure 31 also shows that the effects of the fence on the wing with flaps were similar to the effects observed on the wing without flaps.

The wing drag characteristics with flaps deflected (fig. 32) showed the same trends as with flaps neutral; that is, some drag reductions were effected in the high lift range by delaying separation and the wing drag with suction was less than the drag with leading-edge flap (ref. 1). When the equivalent pump-power drag coefficient C_{DP} was added to that of the wing, however, the total drag was greater than that for the wing with leading-edge flaps. At a lift coefficient of 1.40 with split flaps deflected, the total drag with $C_Q = 0.00048$ was 12 percent higher than the drag of the same configuration with leading-edge flap. At a lift coefficient of 1.80 with double slotted flaps deflected the total drag with $C_Q = 0.00048$ was 7 percent higher than that for the same configuration with leading-edge flap.

Power Requirements for Porous-Leading-Edge Suction

The power requirements (excluding duct, pump, and exit losses) for porous-leading-edge suction were calculated as follows:

$$\text{Horsepower} = \frac{Q(\Delta p)}{550} = \frac{C_Q S V_0 q_0 C_p}{550}$$

A wing loading of 50 pounds per square foot and standard sea-level air density of 0.002378 slug per cubic foot were assumed in calculating q_0 and V_0 . The wing area used was 306.1 square feet, which corresponds to that of a present-day fighter aircraft of similar sweepback angle.

The power requirements were calculated for the flow coefficients obtained in the tests and the duct pressure coefficients required to maintain those flow coefficients through the angle-of-attack range. The calculations were made for several trailing-edge-flap configurations with a porous leading edge from 0 to 0.015c and 0.45b/2 to 0.95b/2 and are presented in figure 33.

The calculations show that the plain wing would require 109 horsepower to maintain a C_Q of 0.00052 (the maximum obtained) through the

stall ($C_p = 49.6$). It would require 24 horsepower to draw a C_Q of 0.00026 (the minimum that produced nose-down moments in the stall) through the stall ($C_p = 20.6$).

With half-span split flaps the wing would require 98 horsepower ($C_p = 59.8$) and with half-span double slotted flaps it would require 78 horsepower ($C_p = 58.1$) to maintain C_Q at 0.00048 beyond $C_{L_{max}}$. This flow rate was sufficient to produce nose-down moments at $C_{L_{max}}$ when the split flaps were deflected but not when the double slotted flaps were deflected. The suction, however, was as effective as a leading-edge flap or slat (ref. 1) in improving the pitching-moment characteristics of the wing with double slotted flaps. These improvements might have been obtained with a lower value of C_Q and consequently lower power but no data were obtained to determine the minimum requirements.

SUMMARY OF RESULTS

The results of an investigation of the effects of drawing air through a porous skin on the leading edge of a 37° sweptback wing of aspect ratio 6 indicate that at low Mach numbers the outboard stall of the wing can be delayed and nose-down moments can be produced at maximum lift about as effectively by that means as was done with a leading-edge flap or slat in a previous investigation on the same wing. The pitching-moment data for the wing with suction, however, indicated a nose-up tendency just prior to the maximum lift coefficient $C_{L_{max}}$ that was not noted in the data for the wing with leading-edge flap or slat.

Suction on either the forward 1 percent of the outer 37 percent of the semispan or the forward $1/2$ percent of the outer 50 percent of the semispan was sufficient to produce stability at the stall. Inboard extension of the 1-percent chordwise extent of porous area increased $C_{L_{max}}$, but extension to include more than the outer 50 percent of the semispan allowed nose-up moments at the stall and did not provide any additional increase in $C_{L_{max}}$. Chordwise extension of the 50-percent semispan extent of porous area from the forward $1/2$ percent to the forward 2 percent of the upper surface increased $C_{L_{max}}$ and further improved the stability at the stall.

The maximum lift coefficient with suction over the outer 50 percent of the semispan ($0.45b/2$ to $0.95b/2$) and the leading $1\frac{1}{2}$ percent of the chord was about 1.33 with flaps neutral, 1.49 with half-span split flap,

and 1.90 with half-span double slotted flap. The pitching-moment data for the configurations with flap neutral and with half-span split flap indicated nose-down moments at $C_{L_{max}}$ although a nose-up tendency was noted just prior to $C_{L_{max}}$; the pitching-moment data for the double slotted flap configuration indicated nose-up moments at $C_{L_{max}}$ but nose-down moments as the lift decreased in the stall.

At Mach numbers above 0.2, stalling occurred over the tip sections of the sealed-leading-edge wing as local sonic velocities were approached. Application of the highest suction-flow rates available ($C_Q = 0.00015$) delayed the tip stall until local velocities of the order of $M_t = 1.20$ were attained but this delay in tip stalling was not sufficient to provide nose-down moments at $C_{L_{max}}$.

Langley Aeronautical Laboratory,
National Advisory Committee for Aeronautics,
Langley Field, Va.

REFERENCES

1. Koven, William, and Graham, Robert R.: Wind-Tunnel Investigation of High-Lift and Stall-Control Devices on a 37° Sweptback Wing of Aspect Ratio 6 at High Reynolds Numbers. NACA RM L8D29, 1948.
2. Salmi, Reino J.: Effects of Leading-Edge Devices and Trailing-Edge Flaps on Longitudinal Characteristics of Two 47.7° Sweptback Wings of Aspect Ratios 5.1 and 6.0 at a Reynolds Number of 6.0×10^6 . NACA RM L50F20, 1950.
3. Pratt, George L., and Shields, E. Rousseau: Low-Speed Longitudinal Characteristics of a 45° Sweptback Wing of Aspect Ratio 8 With High-Lift and Stall-Control Devices at Reynolds Numbers From 1,500,000 to 4,800,000. NACA RM L51J04, 1952.
4. Cook, Woodrow L., and Kelly, Mark W.: The Use of Area Suction for the Purpose of Delaying Separation of Air Flow at the Leading Edge of a 63° Swept-Back Wing - Effects of Controlling the Chordwise Distribution of Suction-Air Velocities. NACA RM A51J24, 1952.
5. Passamanick, Jerome, and Scallion, William I.: The Effects of Suction Through Porous Leading-Edge Surfaces on the Aerodynamic Characteristics of a 47.5° Sweptback Wing-Fuselage Combination at a Reynolds Number of 4.4×10^6 . NACA RM L51K15, 1952.
6. Poppleton, E. D.: Wind Tunnel Tests on a Swept Back Wing Having Distributed Suction on the Leading Edge. TN No. Aero 2081, British R.A.E., Nov. 1950.
7. Sivells, James C., and Deters, Owen J.: Jet-Boundary and Plan-Form Corrections for Partial-Span Models With Reflection Plane, End Plate, or No End Plate in a Closed Circular Wind Tunnel. NACA Rep. 843, 1946. (Supersedes NACA TN 1077.)
8. Eisenstadt, Bertram J.: Boundary-Induced Upwash for Yawed and Swept-Back Wings in Closed Circular Wind Tunnels. NACA TN 1265, 1947.
9. McCullough, George B., and Gault, Donald E.: An Experimental Investigation of the NACA 63₁-012 Airfoil Section With Leading-Edge and Midchord Suction Slots. NACA TN 2041, 1950.

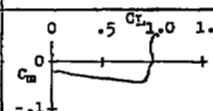
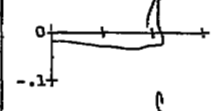
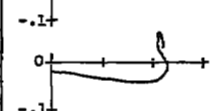
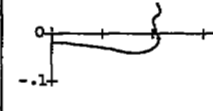
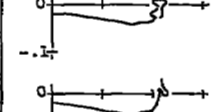
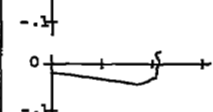
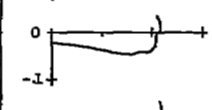
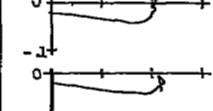
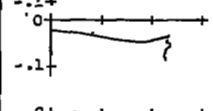
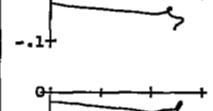
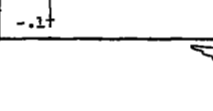
10. Pratt, George L.: Effects of Twist and Camber on the Low-Speed Longitudinal Stability Characteristics of a 45° Sweptback Wing of Aspect Ratio 8 at Reynolds Numbers From 1.5×10^6 to 4.8×10^6 As Determined by Pressure Distributions, Force Tests, and Calculations. NACA RM L52J03a, 1952.
11. Lippisch, A., and Beuschausen, W.: Pressure Distribution Measurements at High Speed and Oblique Incidence of Flow. NACA TM 1115, 1947.
12. Edwards, George G., and Boltz, Frederick W.: An Analysis of the Forces and Pressure Distribution on a Wing With the Leading Edge Swept Back 37.25° . NACA RM A9K01, 1950.

TABLE I.- RATIO OF TOTAL WING AREA TO WING AREA AFFECTED
BY SUCTION FOR THE VARIOUS SPANWISE EXTENTS
OF POROSITY

Spanwise extent of porosity	s/s*
0.15b/2 to 0.95b/2	1.290
0.20b/2 to 0.95b/2	1.400
0.25b/2 to 0.95b/2	1.526
0.30b/2 to 0.95b/2	1.674
0.35b/2 to 0.95b/2	1.847
0.45b/2 to 0.95b/2	2.301
0.58b/2 to 0.95b/2	3.223
0.70b/2 to 0.95b/2	5.092

The NACA logo consists of the letters "NACA" in a bold, sans-serif font, centered within a stylized wing shape that tapers at both ends.

TABLE II.- SUMMARY OF RESULTS OF INVESTIGATION OF SMOKE CONTROL BY LEADING-EDGE SUCTION ON A 17° SWEEPBACK WING

Extent of porous area		Porosity (a)	C _Q	Flap	R × 10 ⁻⁶	M	C _{Lmax}	α at C _{Lmax}	C _m characteristics	Figure No.
Sparwise	Chordwise									
sealed	—	—	—	off	2.50	0.10	1.04	20.3°		6
sealed	—	—	—	off	4.36	.08	1.11	16.3°		6
sealed	—	—	—	off	5.30	.10	1.12	16.4°		6
sealed	—	—	—	off	6.80	.12	1.15	18.4°		6
sealed	—	—	—	off	8.10	.15	1.13	17.4°		6
sealed	—	—	—	off	3.46	.14	1.06	15.3°		8
sealed	—	—	—	off	4.51	.18	1.13	18.1°		8
sealed	—	—	—	off	4.95	.20	1.13	19.4°		8
sealed	—	—	—	off	5.43	.22	1.08	17.3°		8
sealed	—	—	—	off	5.84	.24	1.09	19.3°		8
sealed	—	—	—	off	6.37	.26	1.09	20.3°		8
0.70 b/2 to 0.95 b/2	0 to 0.01c	B	0.00014	off	6.80	.12	1.13	17.4°		11
0.58 b/2 to 0.95 b/2	0 to 0.01c	B	.00021	off	6.80	.12	1.17	20.4°		11
0.45 b/2 to 0.95 b/2	0 to 0.01c	B	.00030	off	6.80	.12	1.30	26.6°		11
0.35 b/2 to 0.95 b/2	0 to 0.01c	B	.00036	off	6.80	.12	1.29	24.6°		11

* See figure 5.

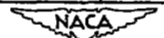
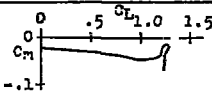
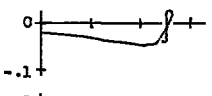
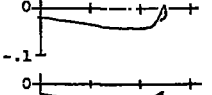
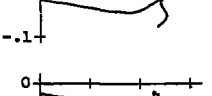
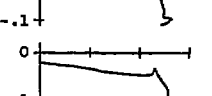
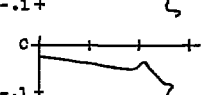
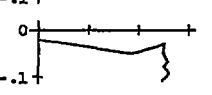
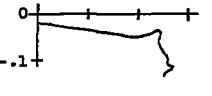
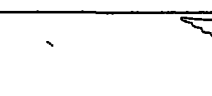


TABLE II.- SUMMARY OF RESULTS OF INVESTIGATION OF STALL CONTROL BY LEADING-EDGE
 SECTION ON A 57° SWEEPBACK WING - Continued

Extent of porous area		Porosity (a)	C_Q	Flap	$R \times 10^{-6}$	M	$C_{L_{max}}$	α at $C_{L_{max}}$	C_m characteristics	Figure No.
Spanwise	Chordwise									
0.30 b/2 to 0.95 b/2	0 to 0.01c	B	.00042	off	6.80	.12	1.27	23.5°		11
0.25 b/2 to 0.95 b/2	0 to 0.01c	B	.00045	off	6.80	.12	1.29	24.5°		11
0.15 b/2 to 0.95 b/2	0 to 0.01c	B	.00044	off	6.80	.12	1.25	22.5°		11
0.15 b/2 to 0.95 b/2	0 to 0.0055c	A	.00030	off	6.80	.12	1.29	26.5°		14
0.45 b/2 to 0.95 b/2	0.001c to 0.01c	A	.00030	off	6.80	.12	1.29	25.5°		14
0.45 b/2 to 0.95 b/2	0 to 0.01c	A	.00034	off	6.80	.12	1.26	25.5°		14
0.45 b/2 to 0.95 b/2	0 to 0.0125c	A	.00045	off	6.80	.12	1.33	23.6°		14
0.45 b/2 to 0.95 b/2	0 to 0.015c	A	.00050	off	6.80	.12	1.33	24.6°		14
0.15 b/2 to 0.95 b/2	0 to 0.02c	A	.00068	off	6.80	.12	1.40	25.6°		14
0.45 b/2 to 0.95 b/2	0 to 0.10c	C	.00080	off	6.80	.12	1.34	23.6°		14
0.45 b/2 to 0.95 b/2	0 to 0.015c	A	.00018	off	6.80	.12	1.19	22.4°		16
0.15 b/2 to 0.95 b/2	0 to 0.015c	A	.00026	off	6.80	.12	1.27	24.5°		16
0.45 b/2 to 0.95 b/2	0 to 0.025c	A	.00040	off	6.80	.12	1.31	24.5°		16
0.45 b/2 to 0.95 b/2	0 to 0.015c	A	.00052	off	6.80	.12	1.33	24.6°		16
0.45 b/2 to 0.95 b/2	0 to 0.015c	A	.00070	off	5.30	.10	1.34	25.6°		16

* See figure 5.

NACA

TABLE II.- SUMMARY OF RESULTS OF INVESTIGATION OF STALL CONTROL BY LEADING-EDGE SECTION ON A 37° SWEPTBACK WING - Continued

Extent of porous area		Porosity (a)	C _Q	Flap	R×10 ⁻⁶	M	C _{i,max}	α at C _{i,max}	C _m characteristics	Figure No.
Spanwise	Chordwise									
0.45 b/2 to 0.95 b/2	0 to 0.015c	A	0.00090	off	4.36	0.08	1.34	23.6°		16
0.45 b/2 to 0.95 b/2	0 to 0.015c	A	.00040	off	4.36	.08	1.29	22.5°		18
0.45 b/2 to 0.95 b/2	0 to 0.015c	A	.00040	off	5.30	.10	1.27	22.5°		18
0.45 b/2 to 0.95 b/2	0 to 0.015c	A	.00040	off	8.10	.15	1.29	24.5°		18
0.45 b/2 to 0.95 b/2	0 to 0.015c	A	.00054	off	4.36	.08	1.32	22.5°		19
0.45 b/2 to 0.95 b/2	0 to 0.015c	A	.00050	off	5.30	.10	1.32	24.5°		19
0.45 b/2 to 0.95 b/2	0 to 0.015c	A	.00046	off	6.80	.12	1.31	25.5°		19
^b 0.45 b/2 to 0.95 b/2	0 to 0.015c	A	.00018	off	6.80	.12	1.19	20.4°		---
^b 0.45 b/2 to 0.95 b/2	0 to 0.015c	A	.00030	off	6.60	.12	1.24	21.5°		26
^b 0.45 b/2 to 0.95 b/2	0 to 0.015c	A	.00049	off	6.80	.12	1.33	24.6°		26
0.45 b/2 to 0.95 b/2	0 to 0.015c	A	power failure	off	6.80	.12	1.06	18.3°		---
0.45 b/2 to 0.95 b/2	0 to 0.015c	A	.00026	off	2.50	.10	1.24	21.6°		22
0.45 b/2 to 0.95 b/2	0 to 0.015c	A	.00017	off	3.46	.14	1.19	21.4°		22
0.45 b/2 to 0.95 b/2	0 to 0.015c	A	.00035	off	3.46	.14	1.29	21.6°		18
0.45 b/2 to 0.95 b/2	0 to 0.015c	A	.00015	off	4.51	.16	1.16	20.4°		22

^a See figure 5.

^b Upper surface fence at 0.50 b/2.



TABLE II.- SUMMARY OF RESULTS OF INVESTIGATION OF STALL CONTROL BY LEADING-EDGE
SUCKION ON A 37° SWEEPBACK WING - Concluded

Extent of porous area		Porosity (a)	C_Q	Flap	$P \times 10^{-6}$	M	$C_{L_{MAX}}$	α at $C_{L_{MAX}}$	C_m characteristics	Figure No.
Spanwise	Chordwise									
0.45 b/2 to 0.95 b/2	0 to 0.015c	A	0.00024	off	4.51	0.18	1.19	21.4°		---
0.45 b/2 to 0.95 b/2	0 to 0.015c	A	.00015	off	4.95	.20	1.21	15.8°		22
0.45 b/2 to 0.95 b/2	0 to 0.015c	A	.00022	off	4.95	.20	1.17	19.4°		---
0.45 b/2 to 0.95 b/2	0 to 0.015c	A	.00016	off	5.43	.22	1.11	15.8°		22
0.45 b/2 to 0.95 b/2	0 to 0.015c	A	.00018	off	5.43	.22	1.28	21.4°		---
0.45 b/2 to 0.95 b/2	0 to 0.015c	A	.00015	off	5.84	.24	1.11	17.4°		22
0.45 b/2 to 0.95 b/2	0 to 0.015c	A	.00014	off	6.37	.26	1.10	20.3°		22
sealed	---	---	---	split	6.80	.12	1.36	13.6°		28
0.45 b/2 to 0.95 b/2	0 to 0.015c	A	.00046	split	6.80	.12	1.49	16.8°		28
0.45 b/2 to 0.95 b/2	0 to 0.015c	A	.00046	split	6.80	.12	1.45	15.7°		28
0.45 b/2 to 0.95 b/2	0 to 0.015c	A	.00048	double slotted	6.80	.12	1.90	15.2°		29
0.45 b/2 to 0.95 b/2	0 to 0.015c	A	.00048	double slotted	6.80	.12	1.85	13.2°		29
sealed	---	---	---	double slotted	5.84	.24	1.68	11.0°		30
0.45 b/2 to 0.95 b/2	0 to 0.015c	A	.00016	double slotted	5.84	.24	1.72	11.0°		30

*See figure 5.

†Upper surface fence at 0.50 b/2.

NACA

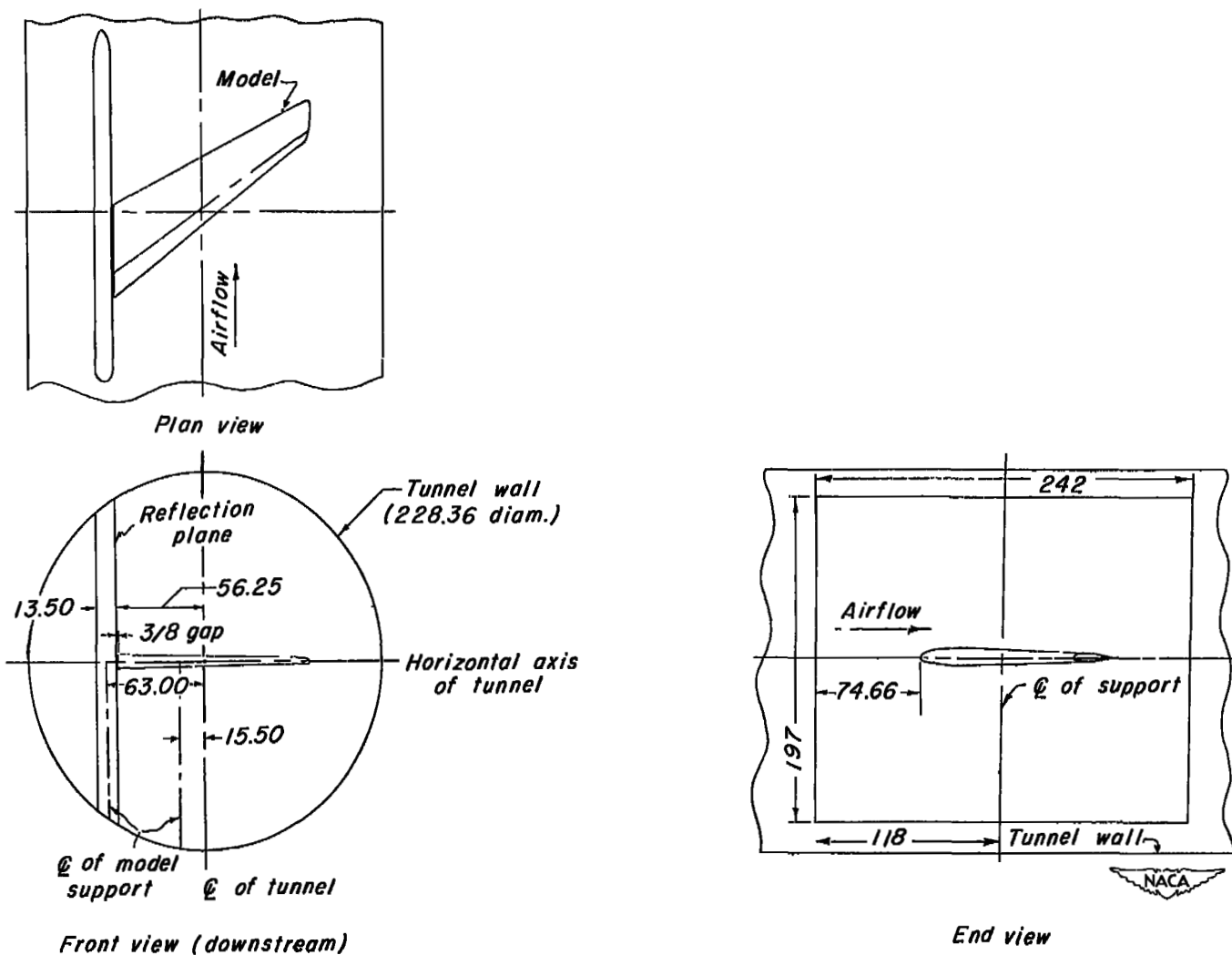


Figure 1.- Details of setup of 37° sweptback semispan wing and reflection plane in Langley 19-foot pressure tunnel. All dimensions are in inches.



Figure 2.- Model and reflection plane in the Langley 19-foot pressure tunnel.

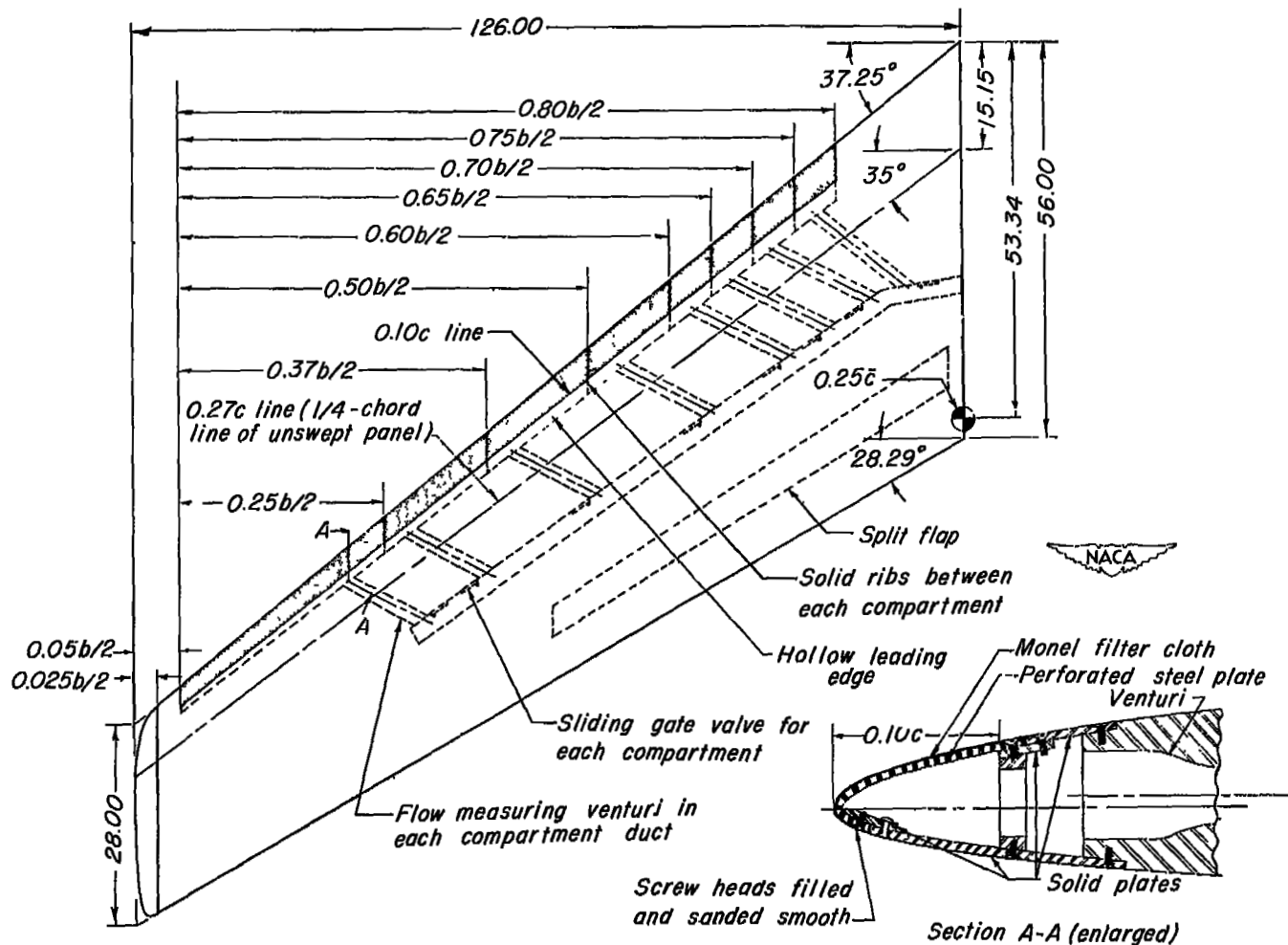


Figure 3.- General layout and internal ducting of model with porous leading-edge surface. Area (complete wing), 73.296 square feet; aspect ratio, 6; taper ratio, 0.5; $\bar{c} = 3.6292$ feet. All dimensions are in inches.

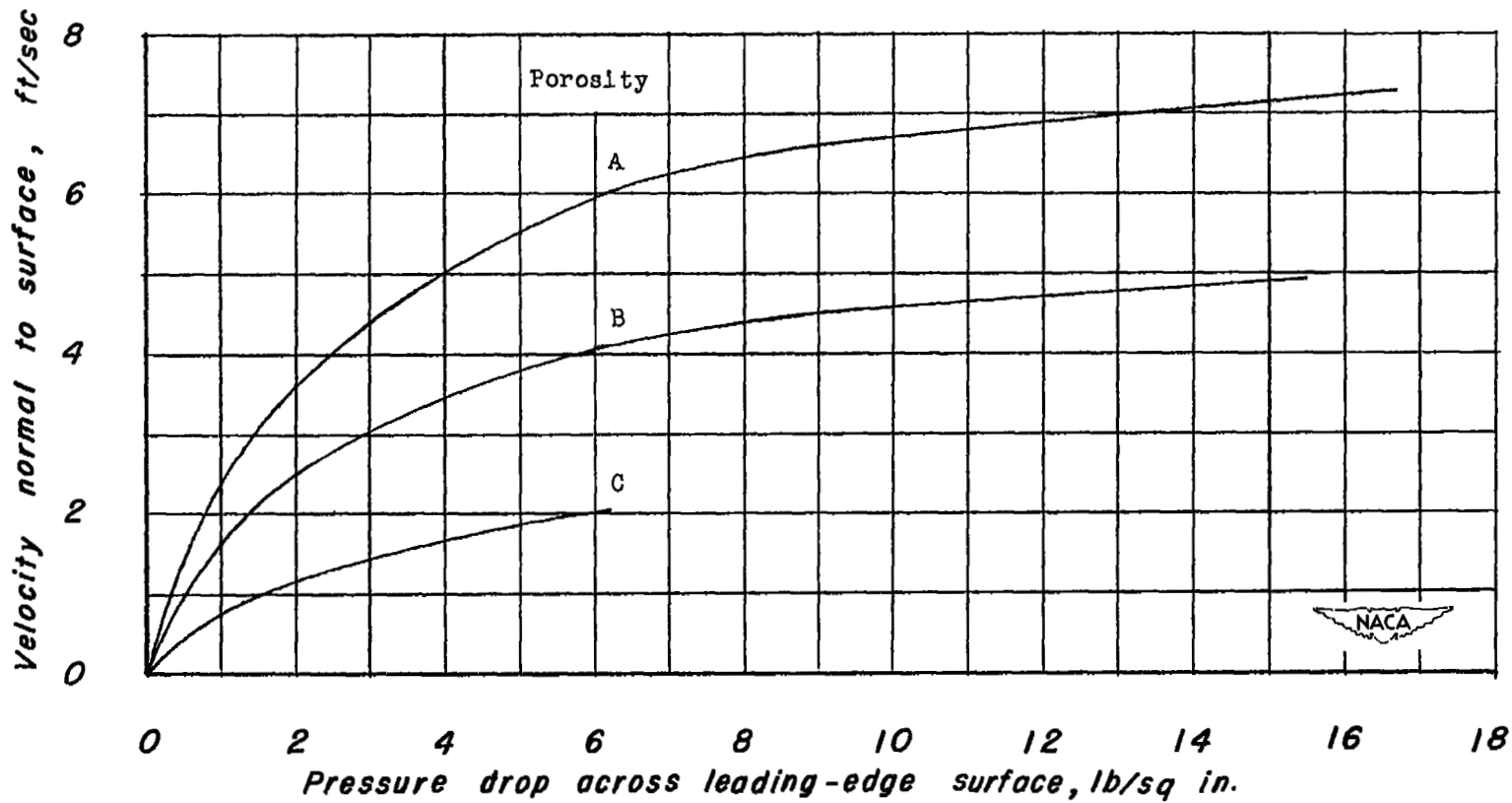


Figure 5.- Porosity characteristics of leading-edge surfaces.

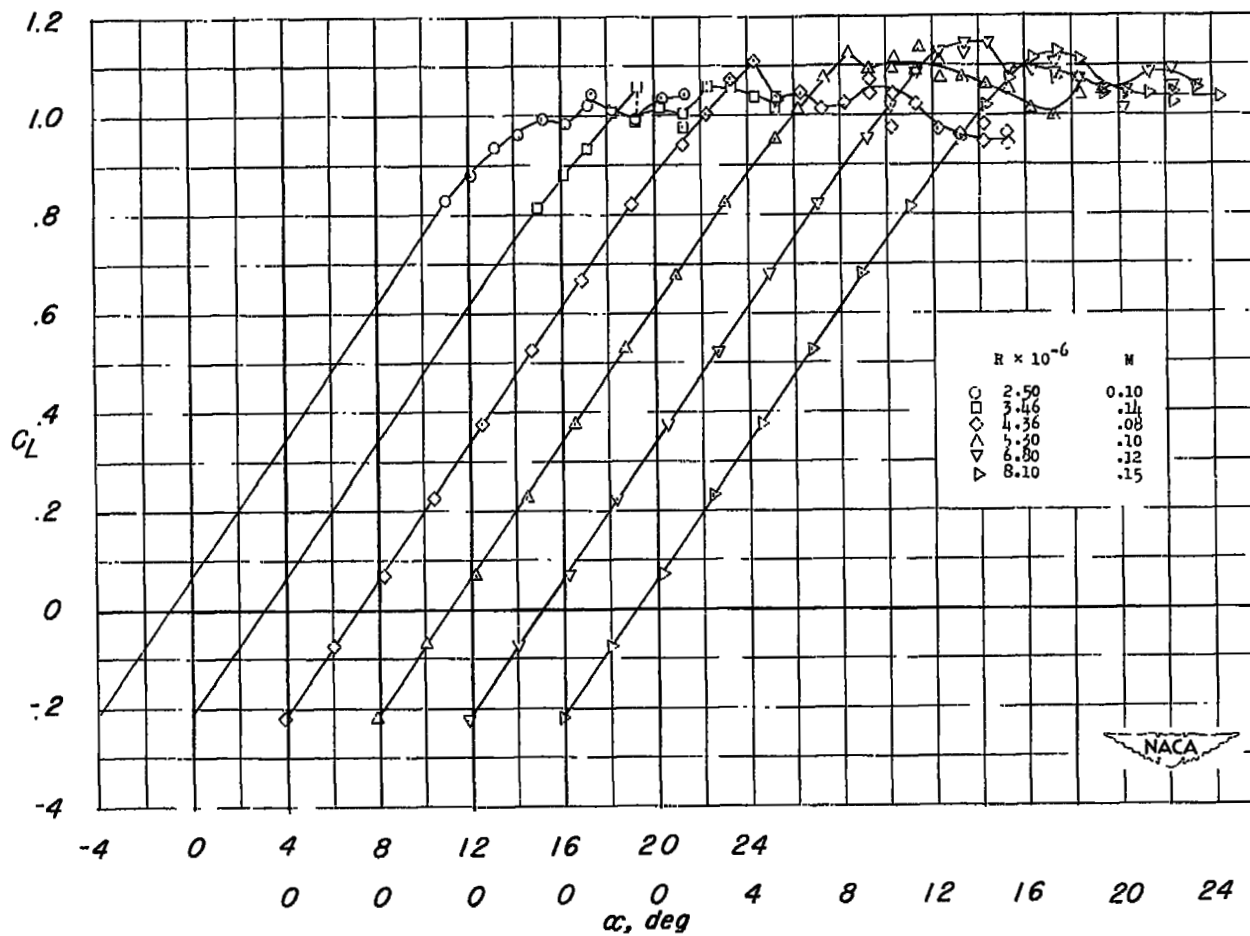
(a) C_L against α .

Figure 6.- Effects of Reynolds number variation on the aerodynamic characteristics of the 37° sweptback wing with porous leading edge sealed.

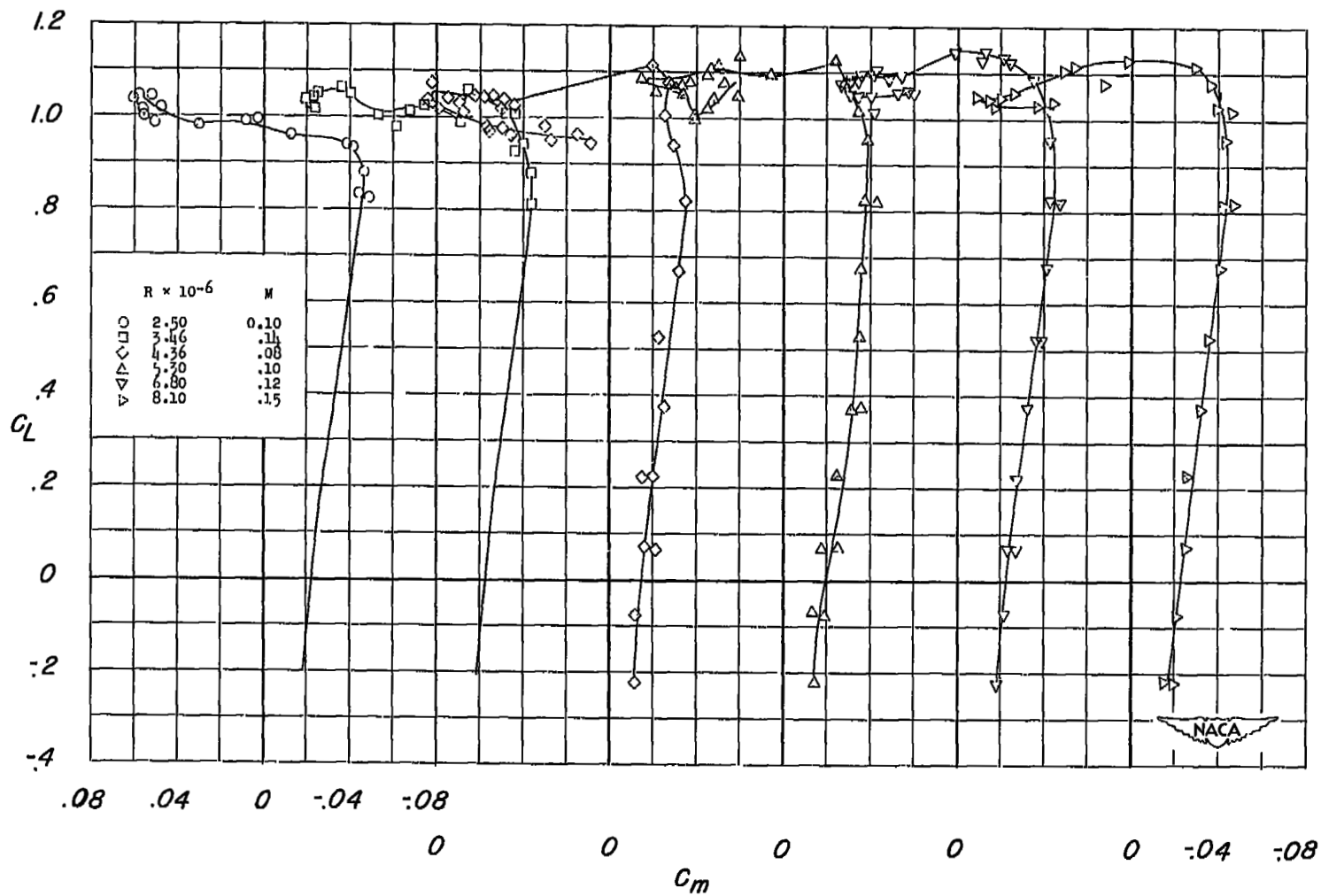
(b) C_L against C_m .

Figure 6.- Concluded.

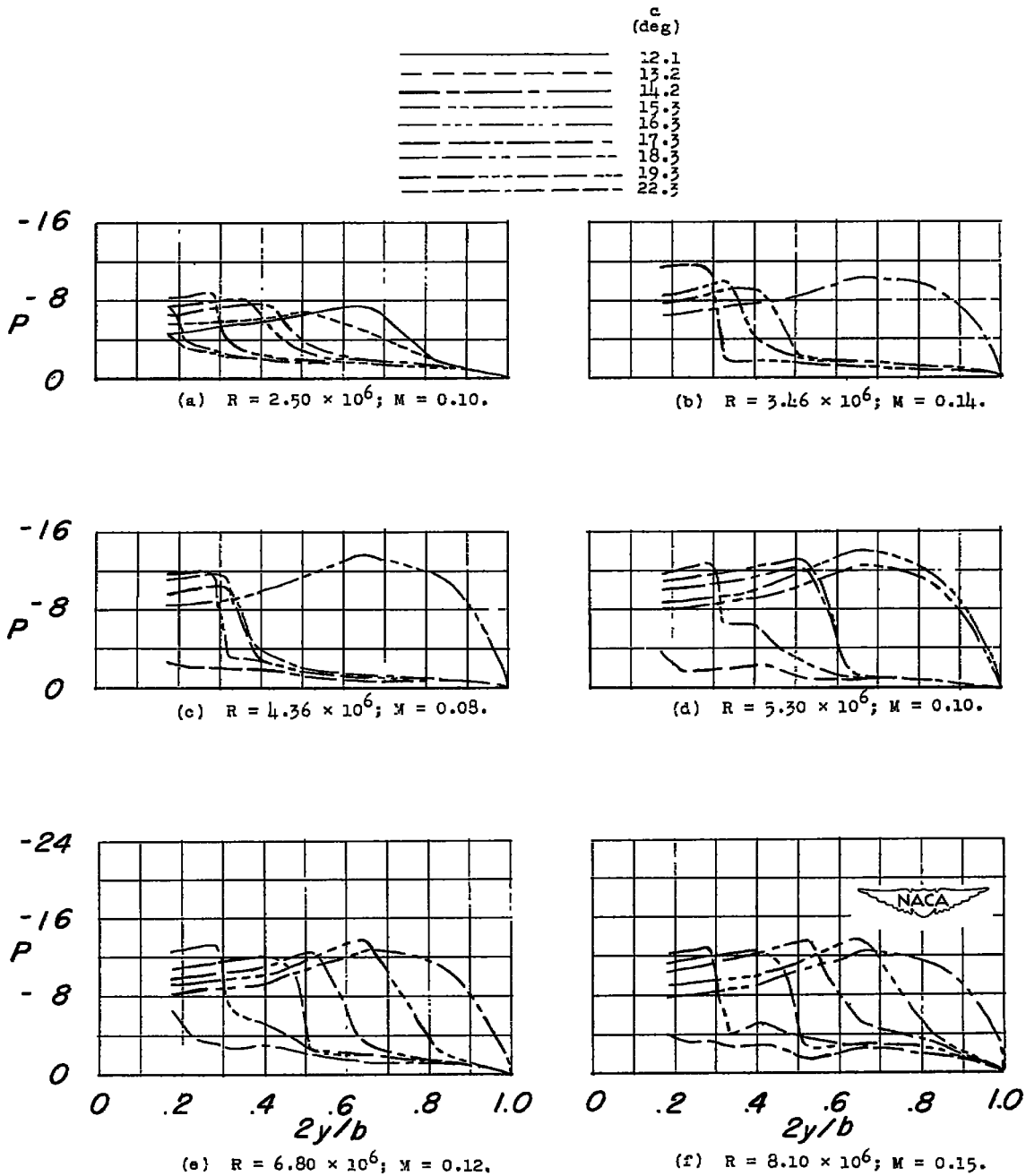
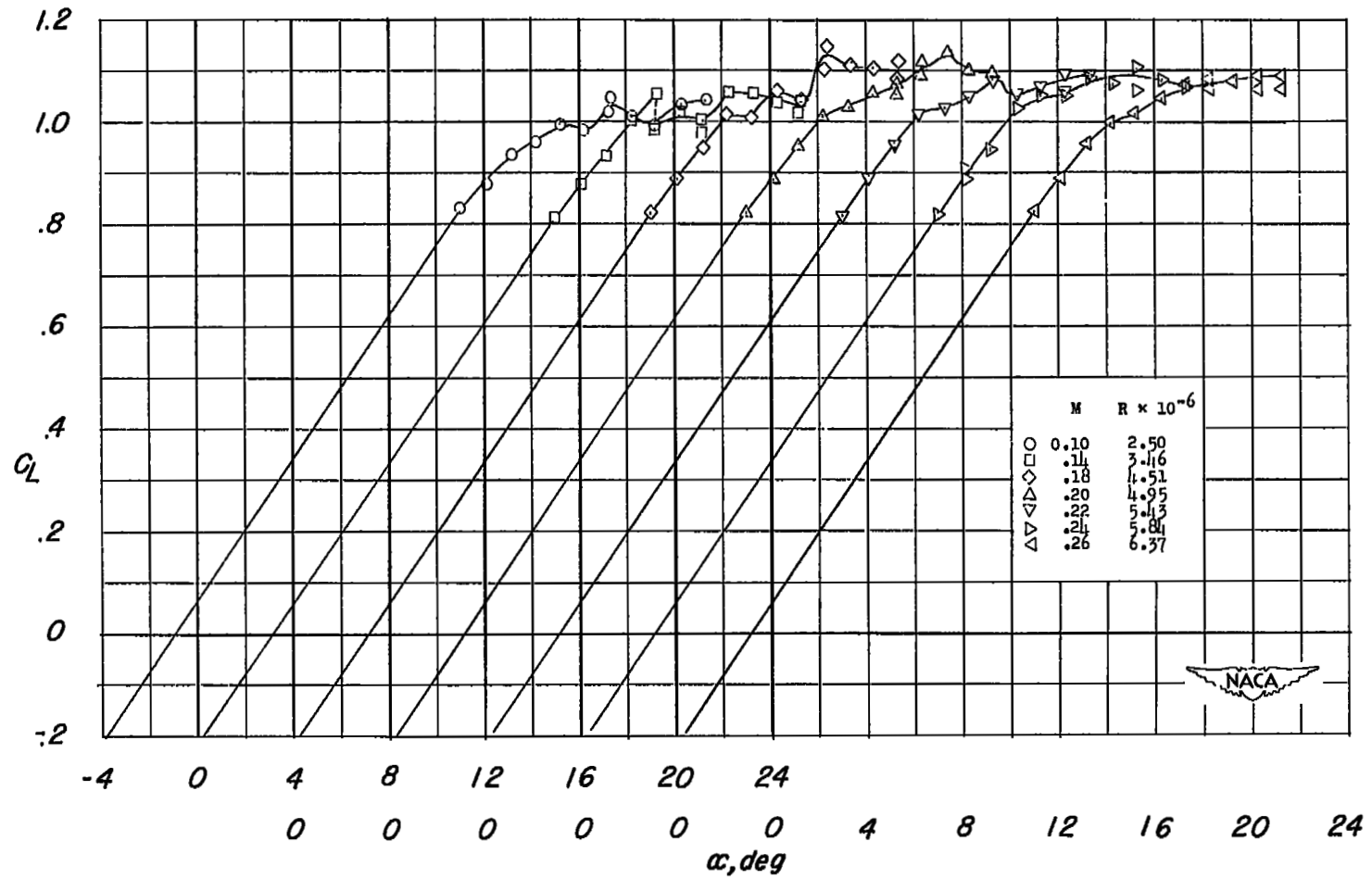
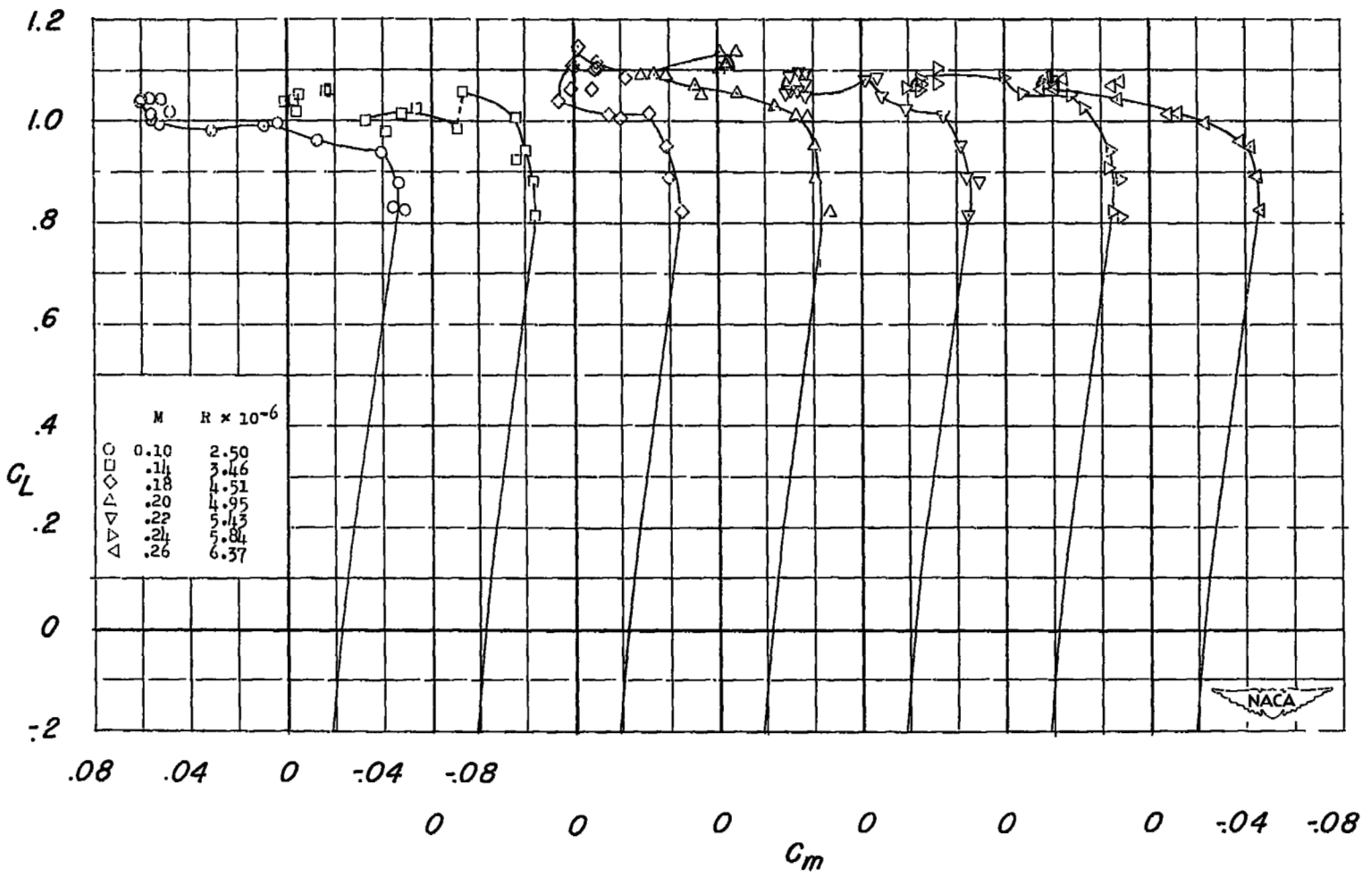


Figure 7.- Effects of Reynolds number variation on the leading-edge pressure coefficients of the 37° sweptback wing with porous leading edge sealed.



(a) C_L against α .

Figure 8.- Effects of Mach number and Reynolds number variation on the aerodynamic characteristics of the 37° sweptback wing with porous leading edge sealed.



(b) C_L against C_m .

Figure 8.- Concluded.

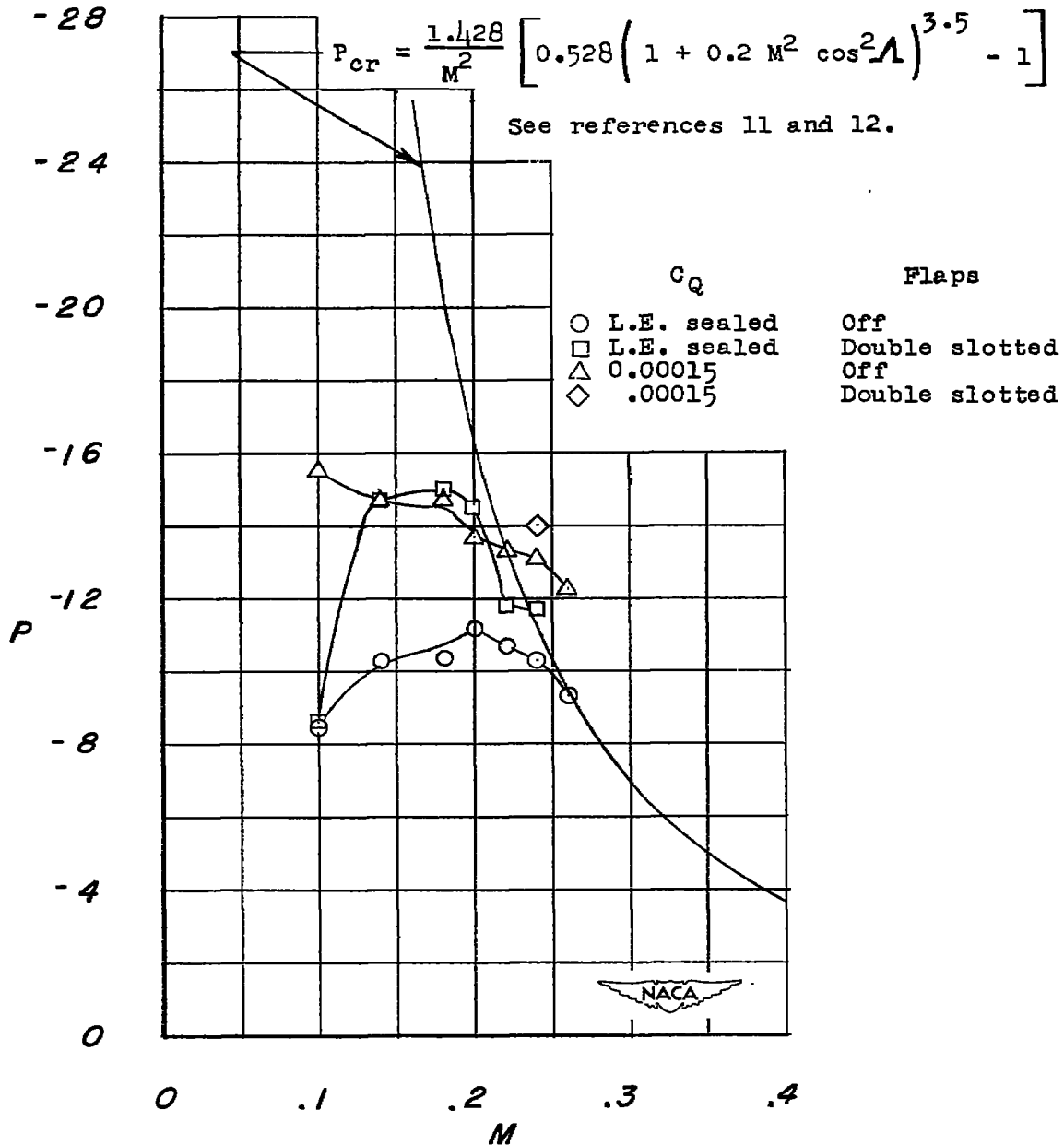


Figure 9.- Variation of peak measured leading-edge pressure coefficients with Mach number. Porosity A; spanwise extent, $0.45b/2$ to $0.95b/2$; chordwise extent, 0 to $0.015c$.

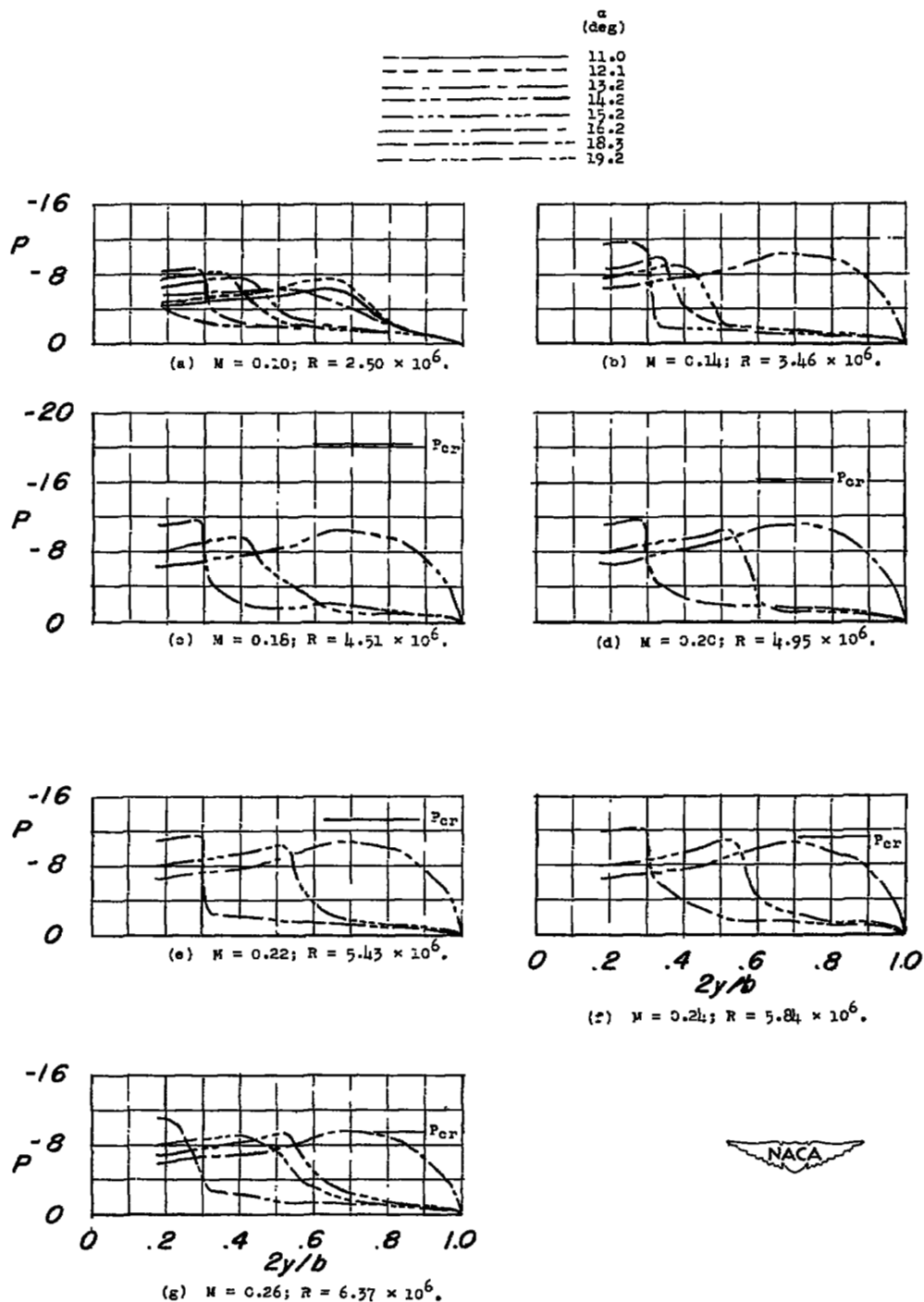
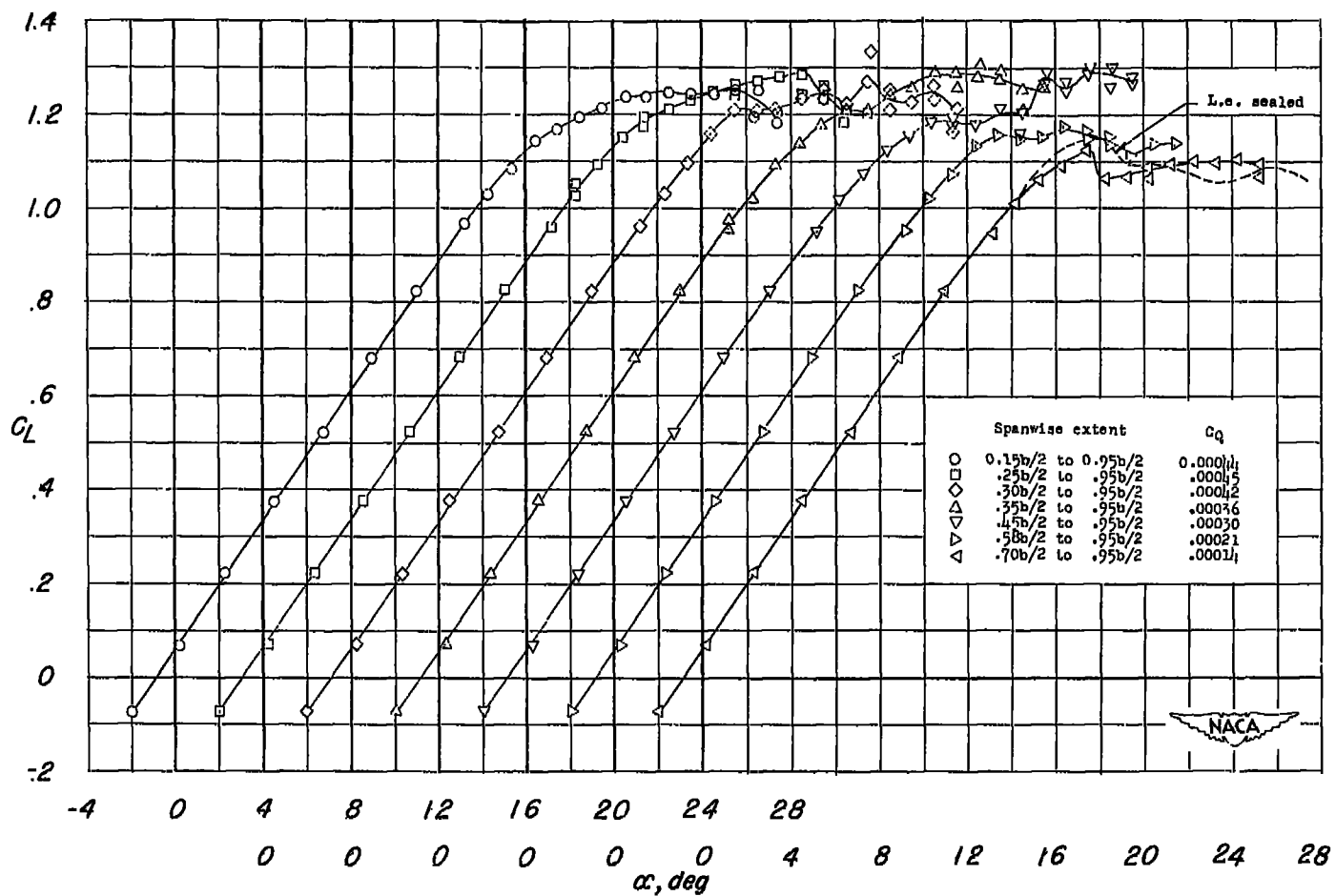
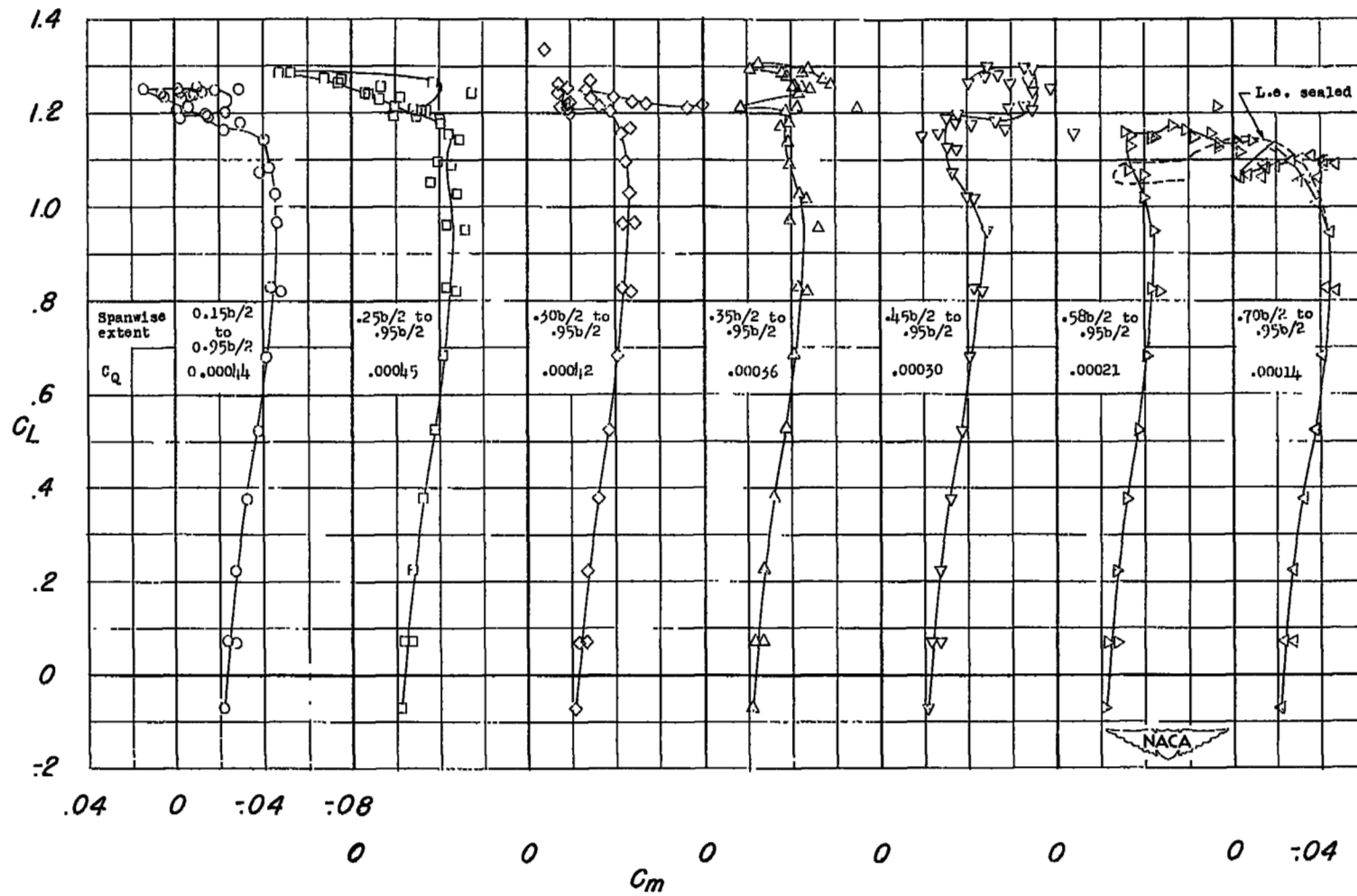


Figure 10.- Effects of Mach number and Reynolds number variation on the leading-edge pressure coefficients of 37° sweptback wing with porous leading edge sealed.



(a) C_L against α .

Figure 11.- Effects of spanwise variation of extent of porous area on the aerodynamic characteristics of the 37° sweptback wing. Porosity B; chordwise extent, 0 to $0.01c$; $R = 6.80 \times 10^6$; $M = 0.12$.



(b) C_L against C_m .

Figure 11.- Concluded.

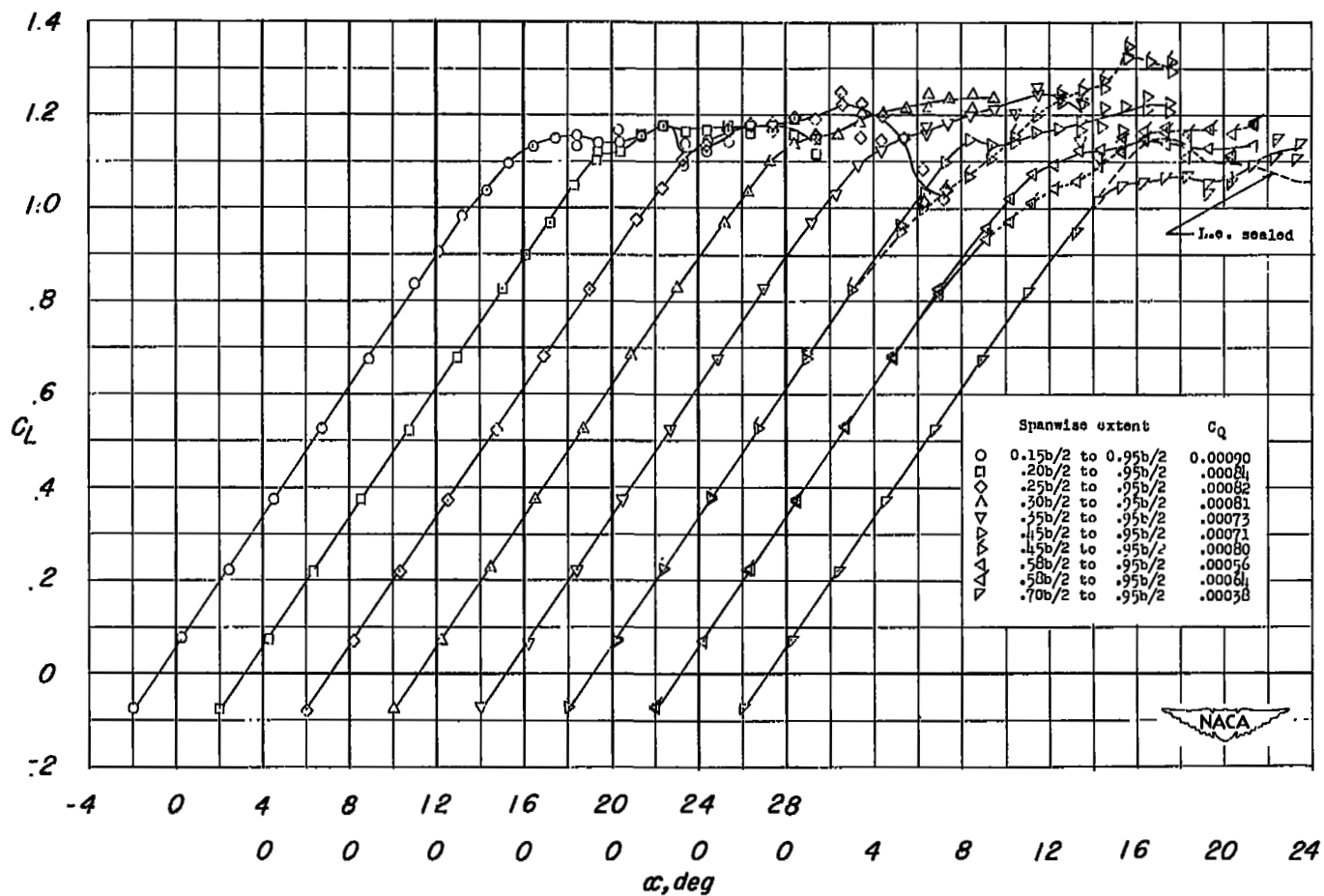
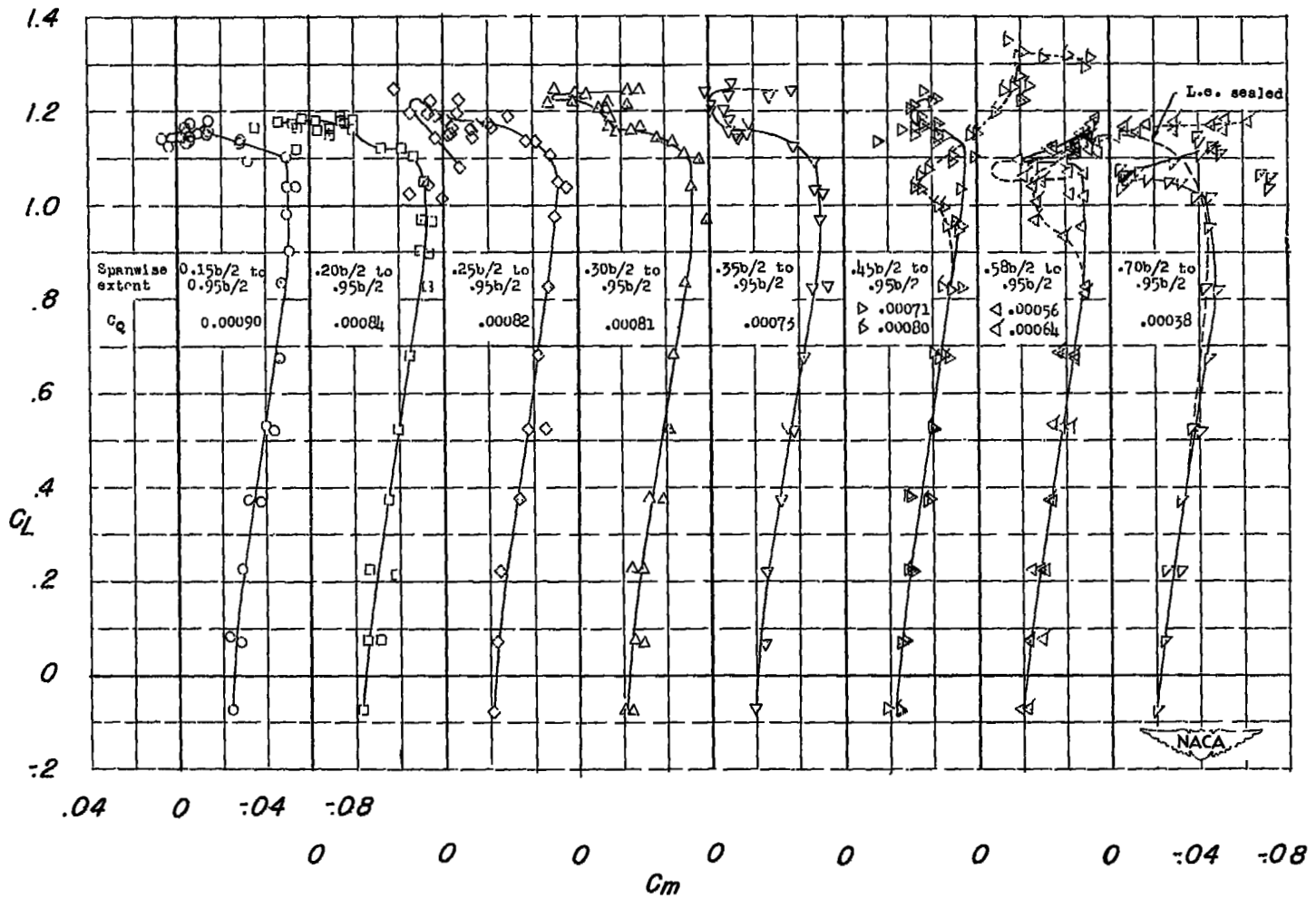
(a) C_L against α .

Figure 12.- Effects of spanwise variation of extent of porous area on the aerodynamic characteristics of the 37° sweptback wing. Porosity C (flagged symbols denote porosity B); chordwise extent, 0 to $0.10c$; $R = 6.80 \times 10^6$; $M = 0.12$.



(b) C_L against C_m .

Figure 12.- Concluded.

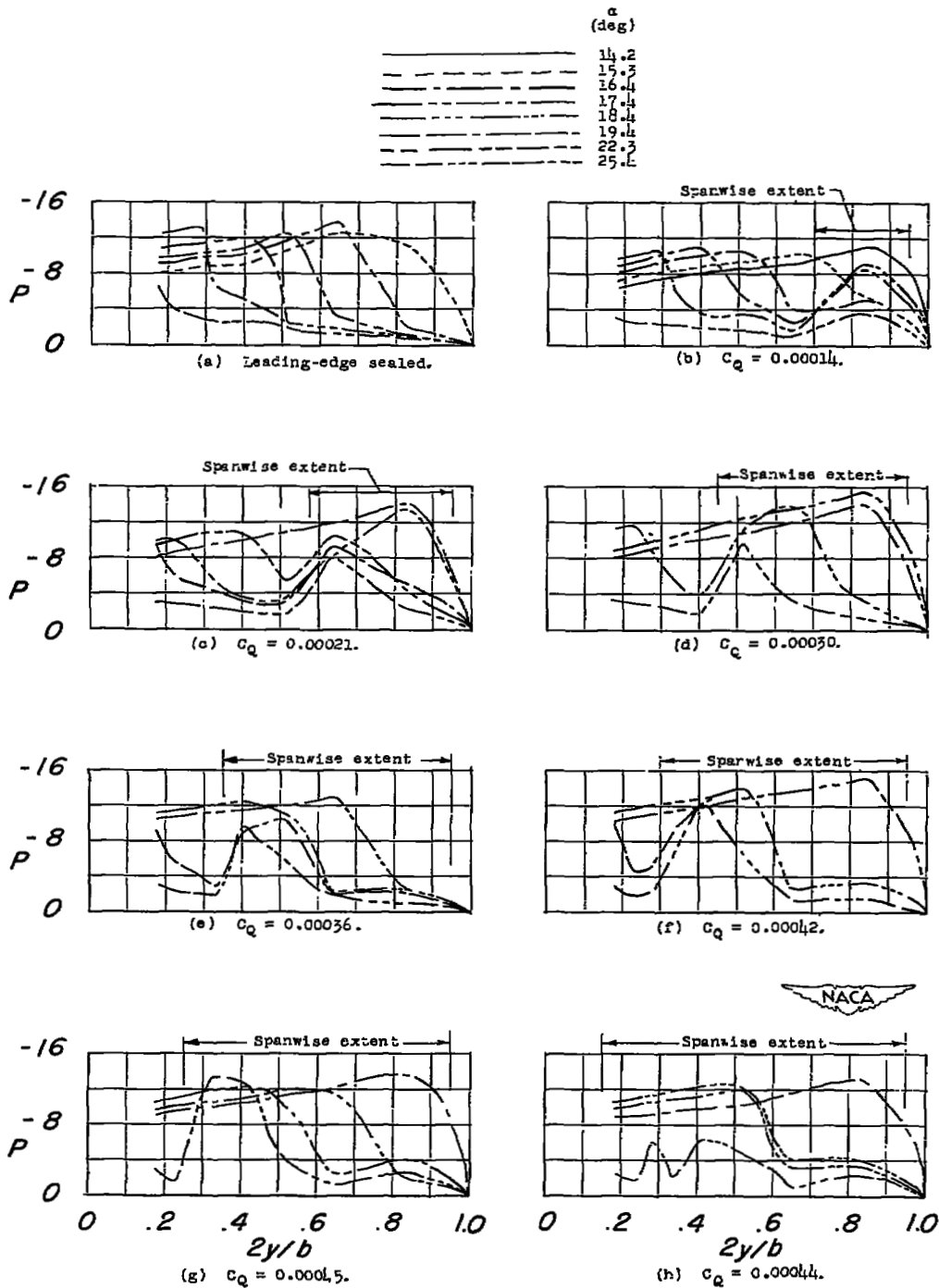


Figure 13.- Effects of spanwise variation of extent of porous area on the leading-edge pressure coefficients of the 37° sweptback wing. Porosity B; chordwise extent, 0 to 0.01c; $R = 6.80 \times 10^6$; $M = 0.12$.

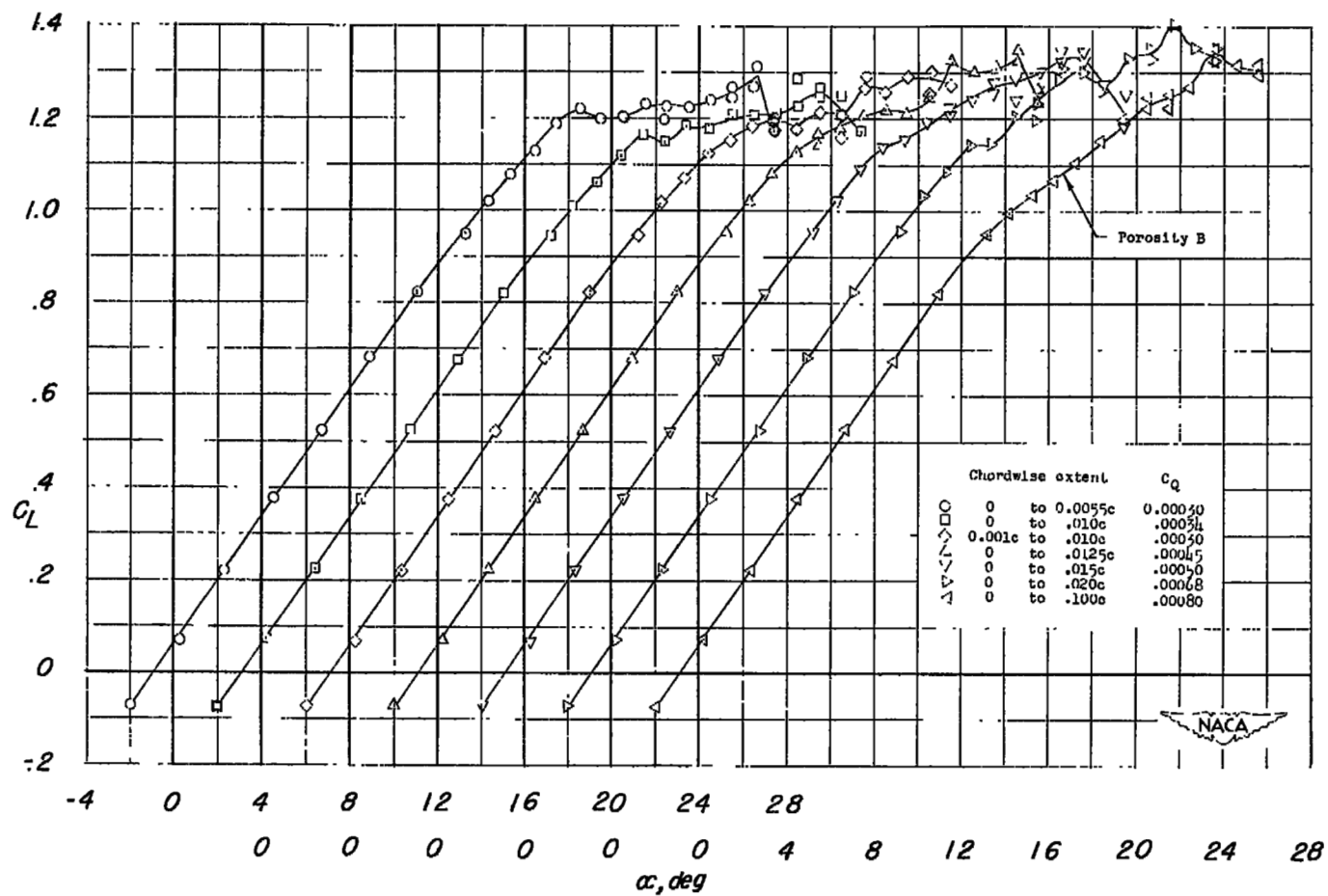
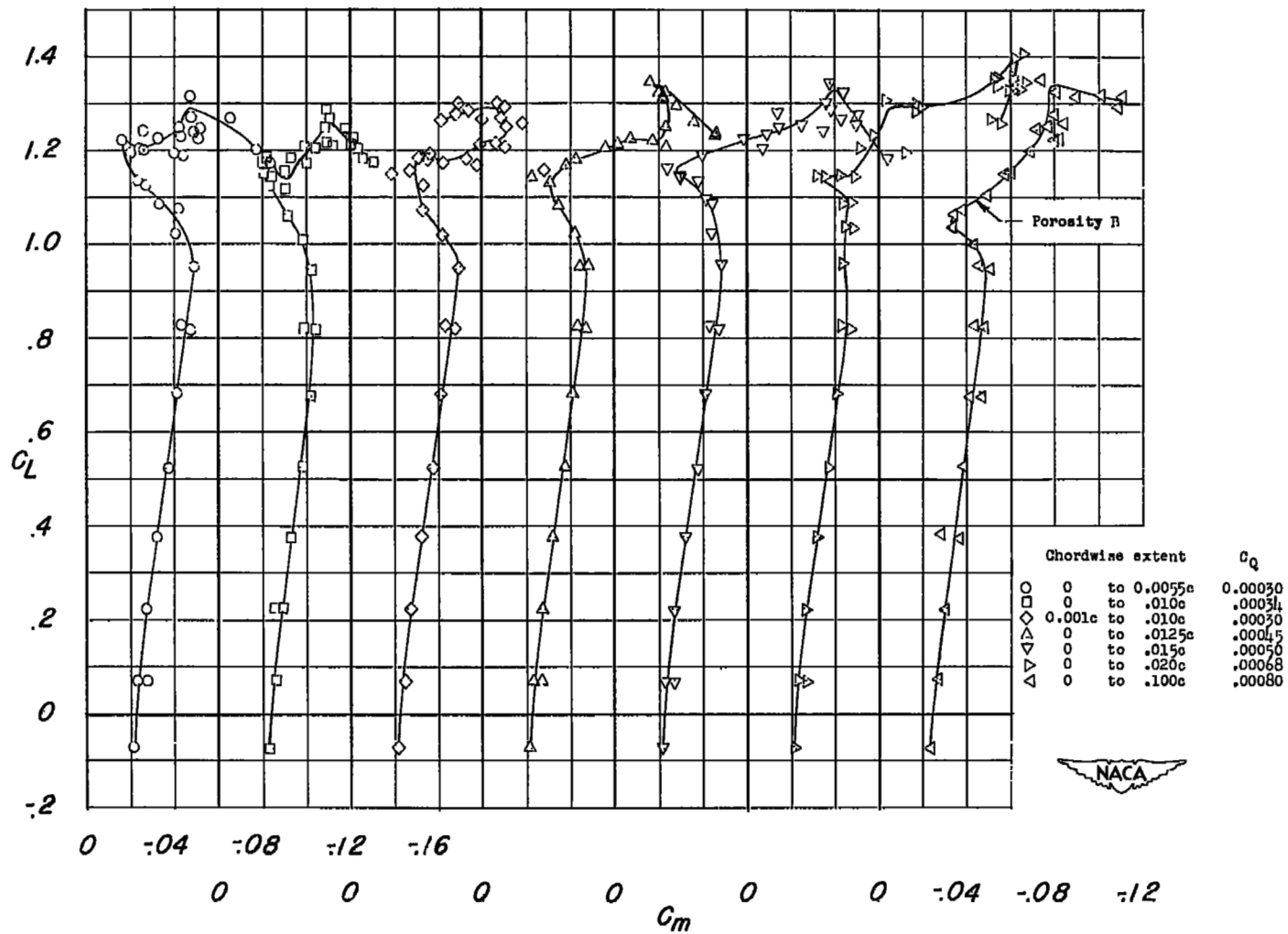
(a) C_L against α .

Figure 14.- Effects of chordwise variation of extent of porous area on the aerodynamic characteristics of the 37° sweptback wing. Porosity A except where noted; spanwise extent, $0.45b/2$ to $0.95b/2$; $R = 6.80 \times 10^6$; $M = 0.12$.



(b) C_L against C_m .

Figure 14.- Concluded.

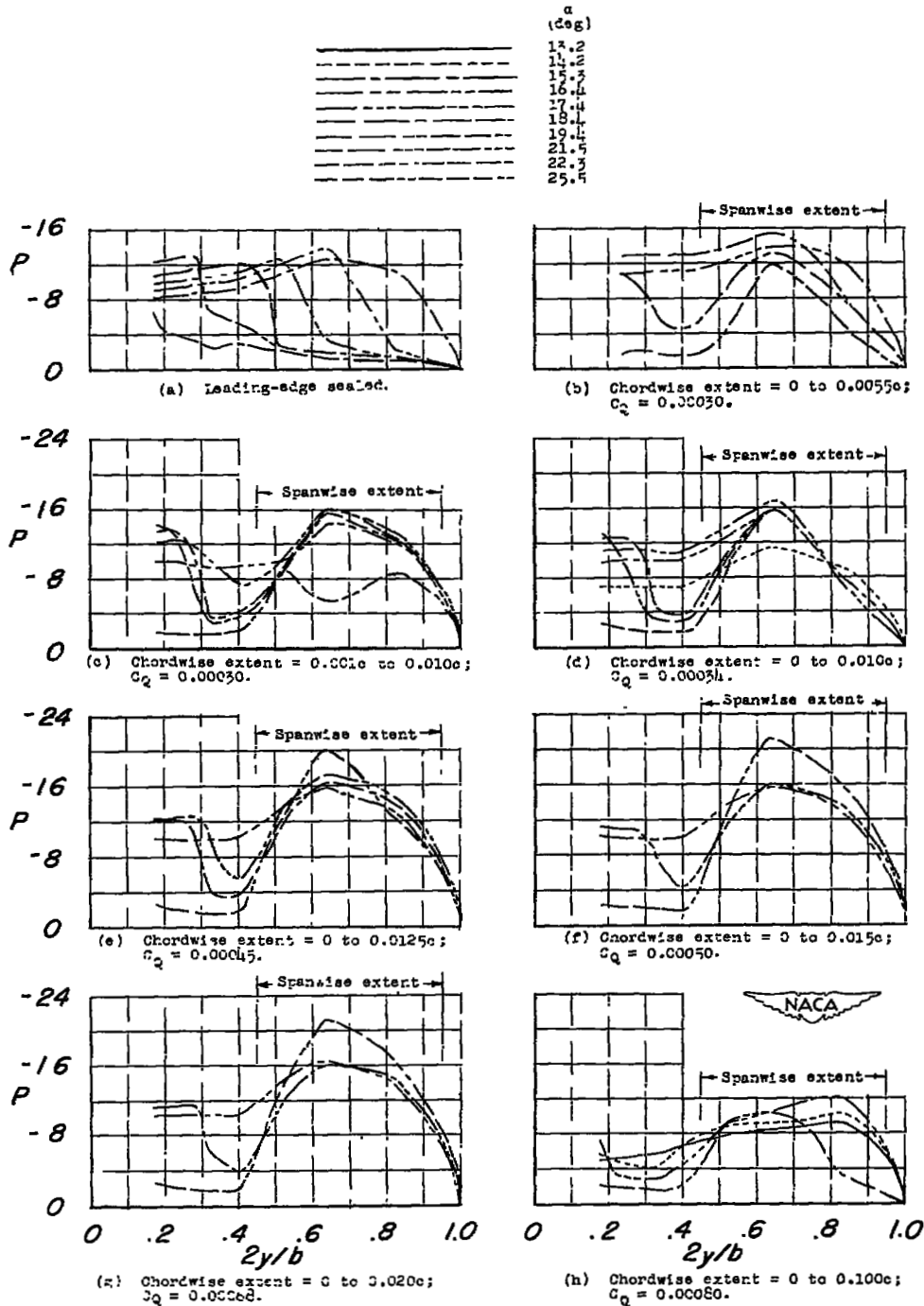


Figure 15.- Effects of chordwise variation of extent of porous area on the leading-edge pressure coefficients of the 37° sweptback wing. Porosity A; spanwise extent, $0.45b/2$ to $0.95b/2$; $R = 6.80 \times 10^6$; $M = 0.12$.

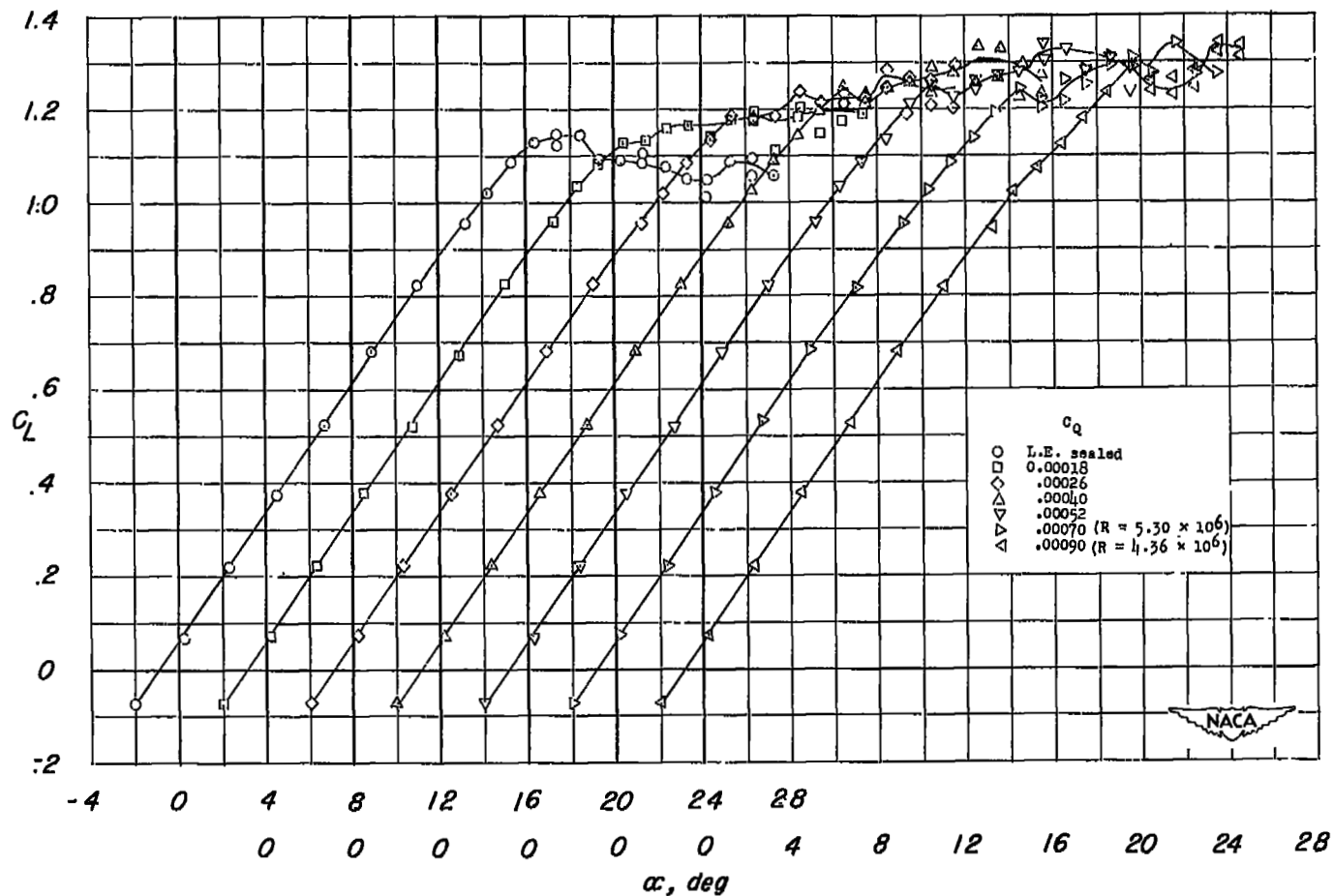
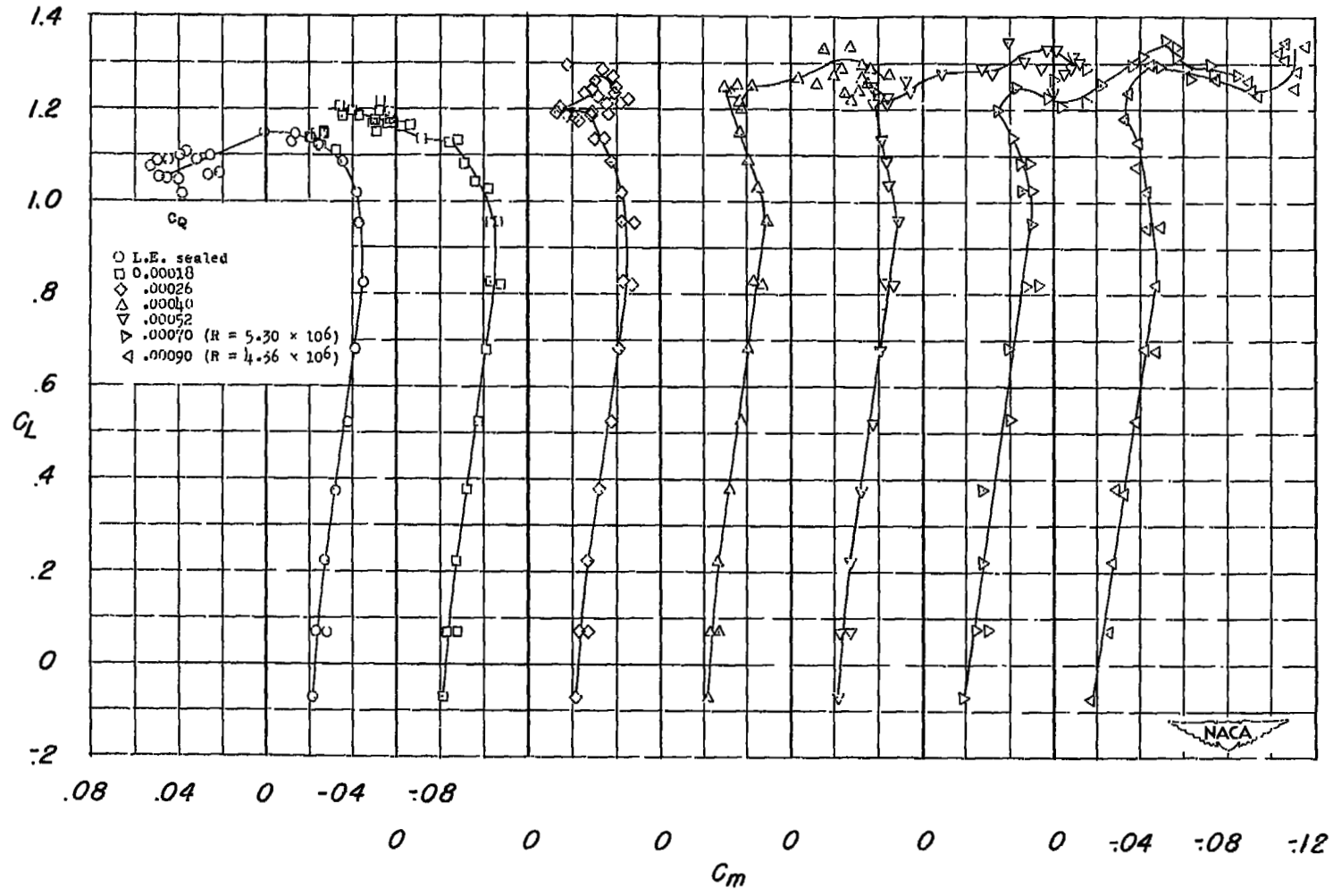
(a) C_L against α .

Figure 16.- Effects of C_Q variation on the aerodynamic characteristics of the 37° sweptback wing. Porosity A; spanwise extent, $0.45b/2$ to $0.95b/2$; chordwise extent, 0 to $0.015c$; $R = 6.80 \times 10^6$; $M = 0.12$.



(b) C_L against C_m .
Figure 16.- Concluded.

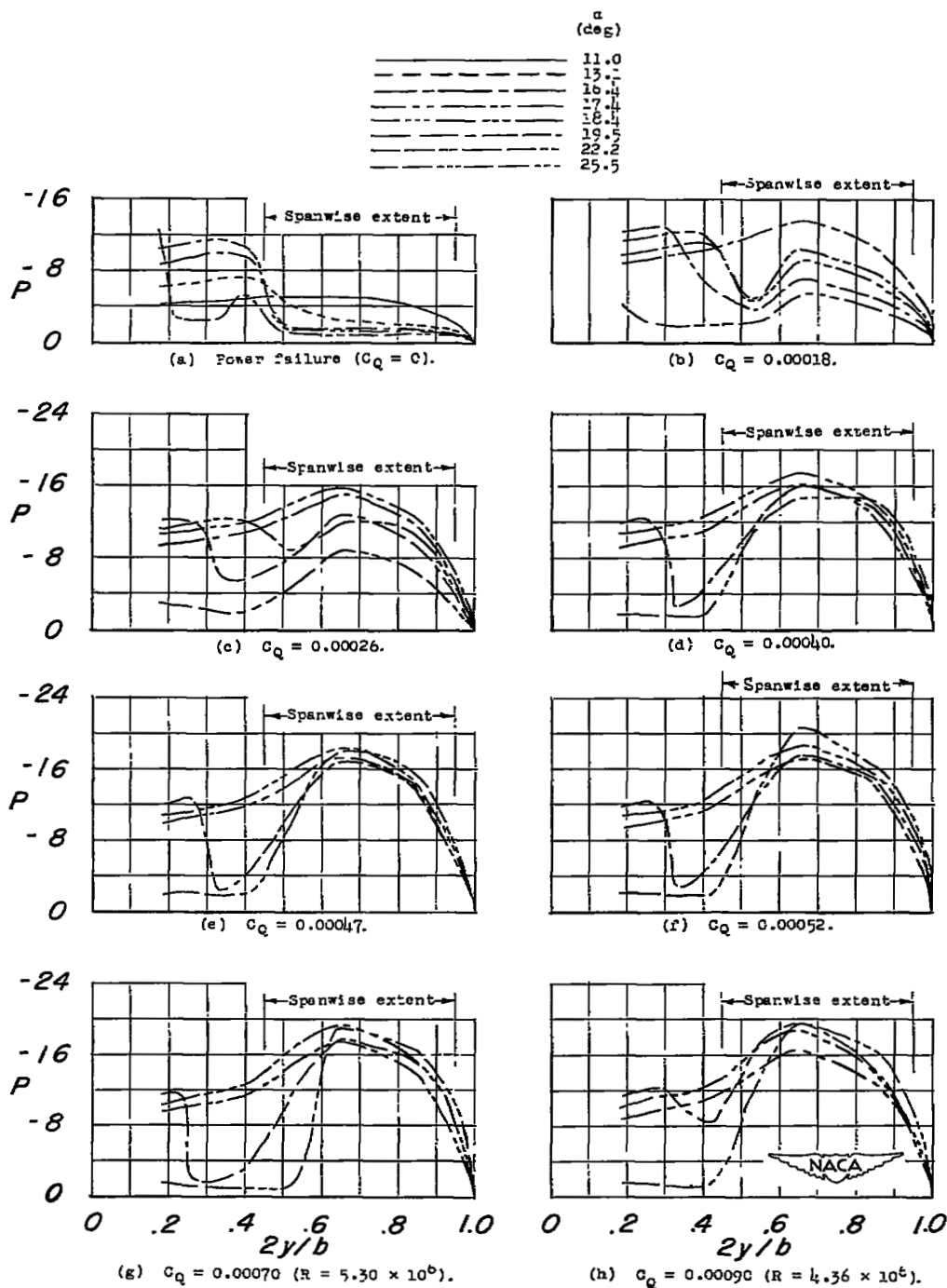
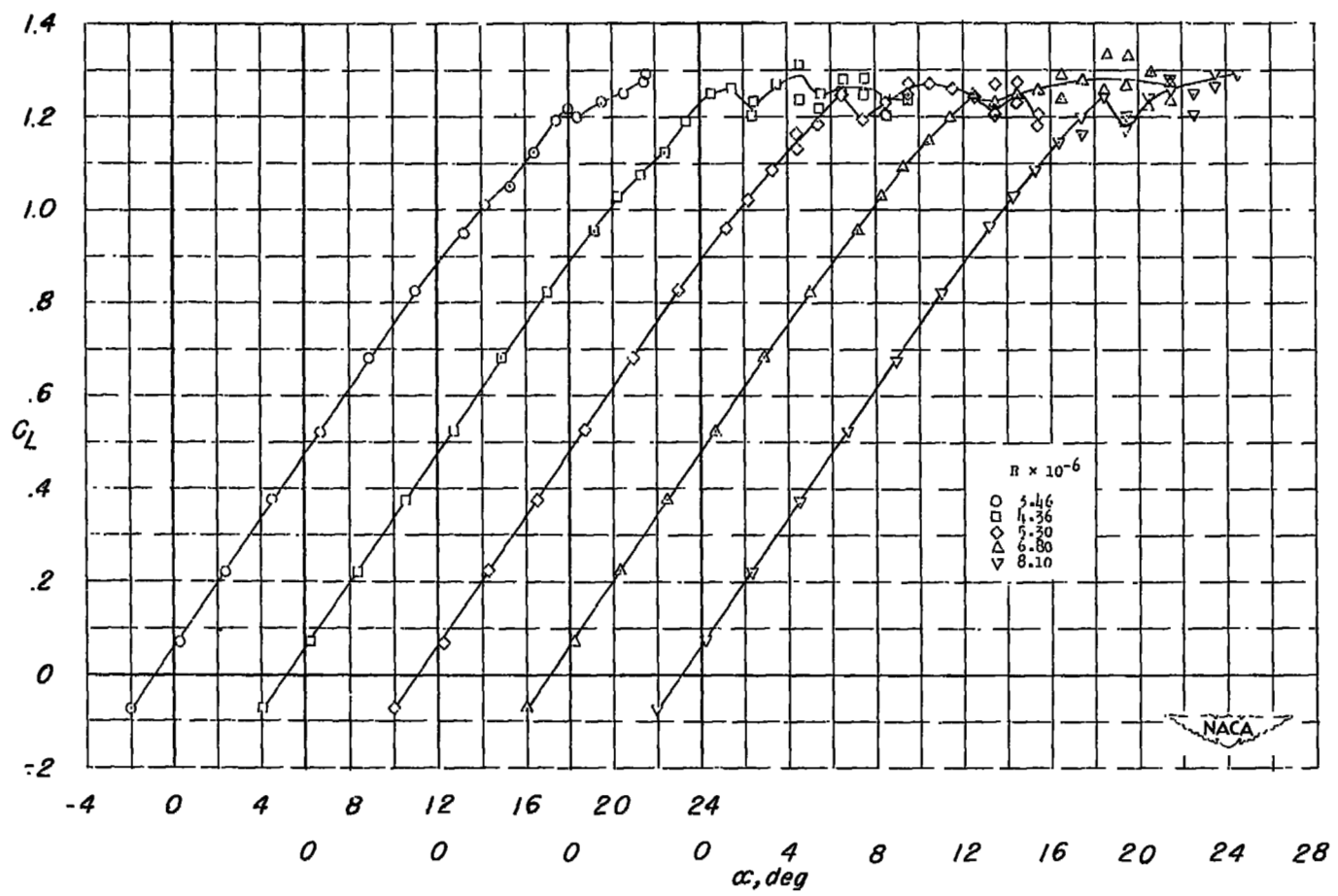
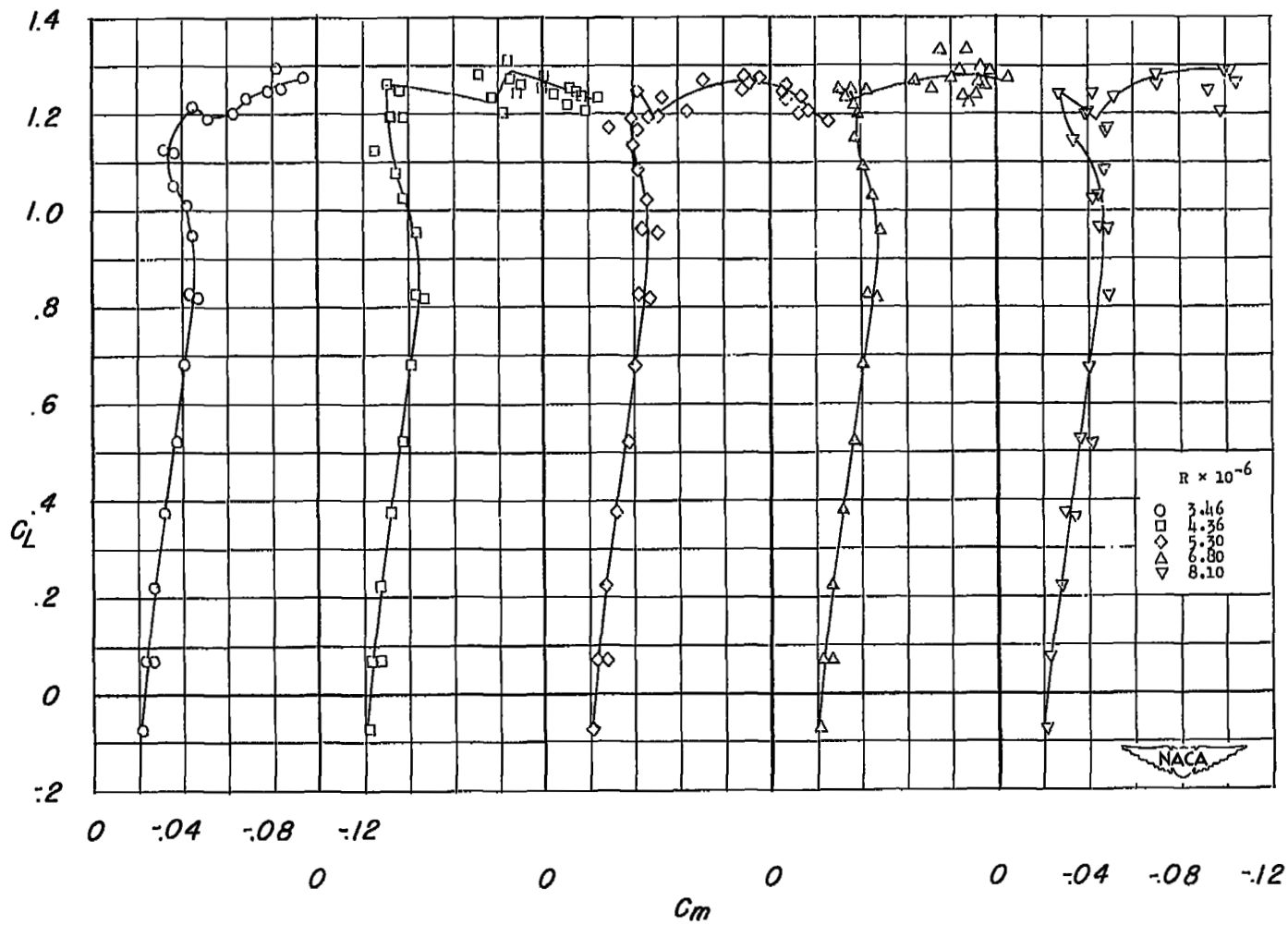


Figure 17.- Effects of C_Q variation on the leading-edge pressure coefficients of the 37° sweptback wing. Porosity A; spanwise extent, $0.45b/2$ to $0.95b/2$; chordwise extent, 0 to $0.015c$; $R = 6.80 \times 10^6$; $M = 0.12$.



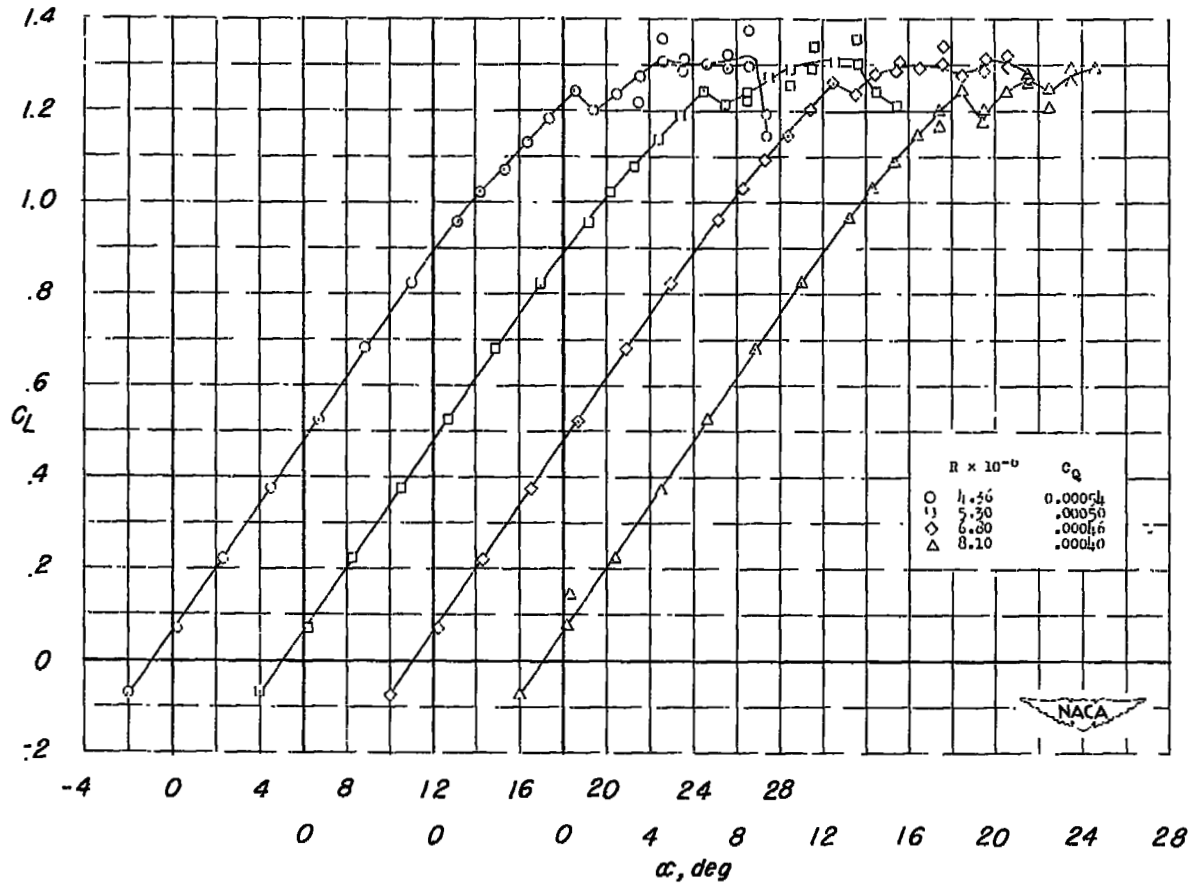
(a) C_L against α .

Figure 18.- Effects of Reynolds number variation on the aerodynamic characteristics of the 37° sweptback wing. Porosity A; spanwise extent, $0.45b/2$ to $0.95b/2$; chordwise extent, 0 to $0.015c$; $C_Q \approx 0.00040$.



(b) C_L against C_m .

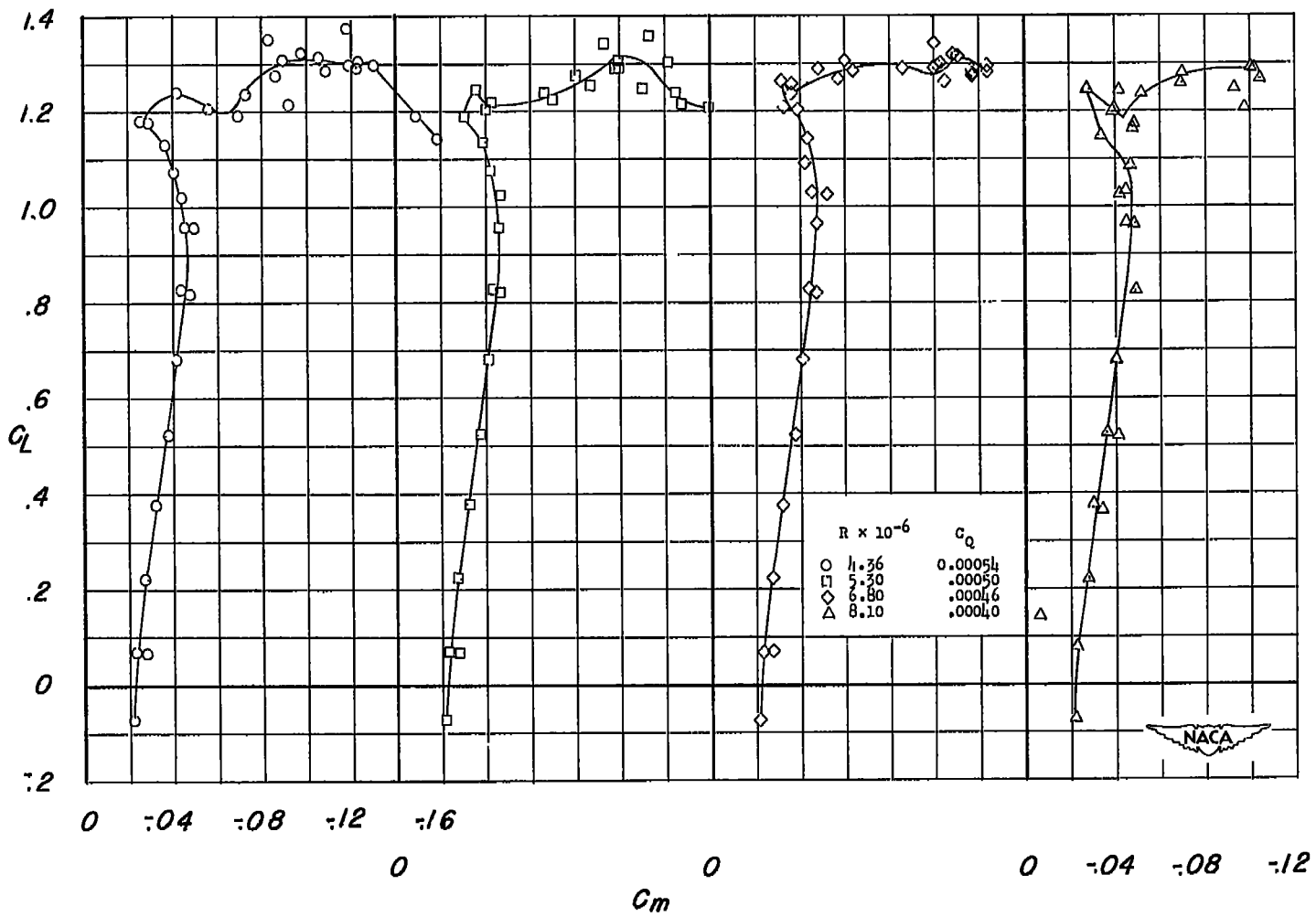
Figure 18.- Concluded.



(a) C_L against α .

Figure 19.- Effects of Reynolds number variation on the aerodynamic characteristics of the 37° sweptback wing. Porosity A; spanwise extent, $0.45b/2$ to $0.95b/2$; chordwise extent, 0 to $0.015c$;

$$C_{QR}^{1/2} \approx 0.00040 \sqrt{8.10 \times 10^6}$$



(b) C_L against C_m .
 Figure 19.- Concluded.

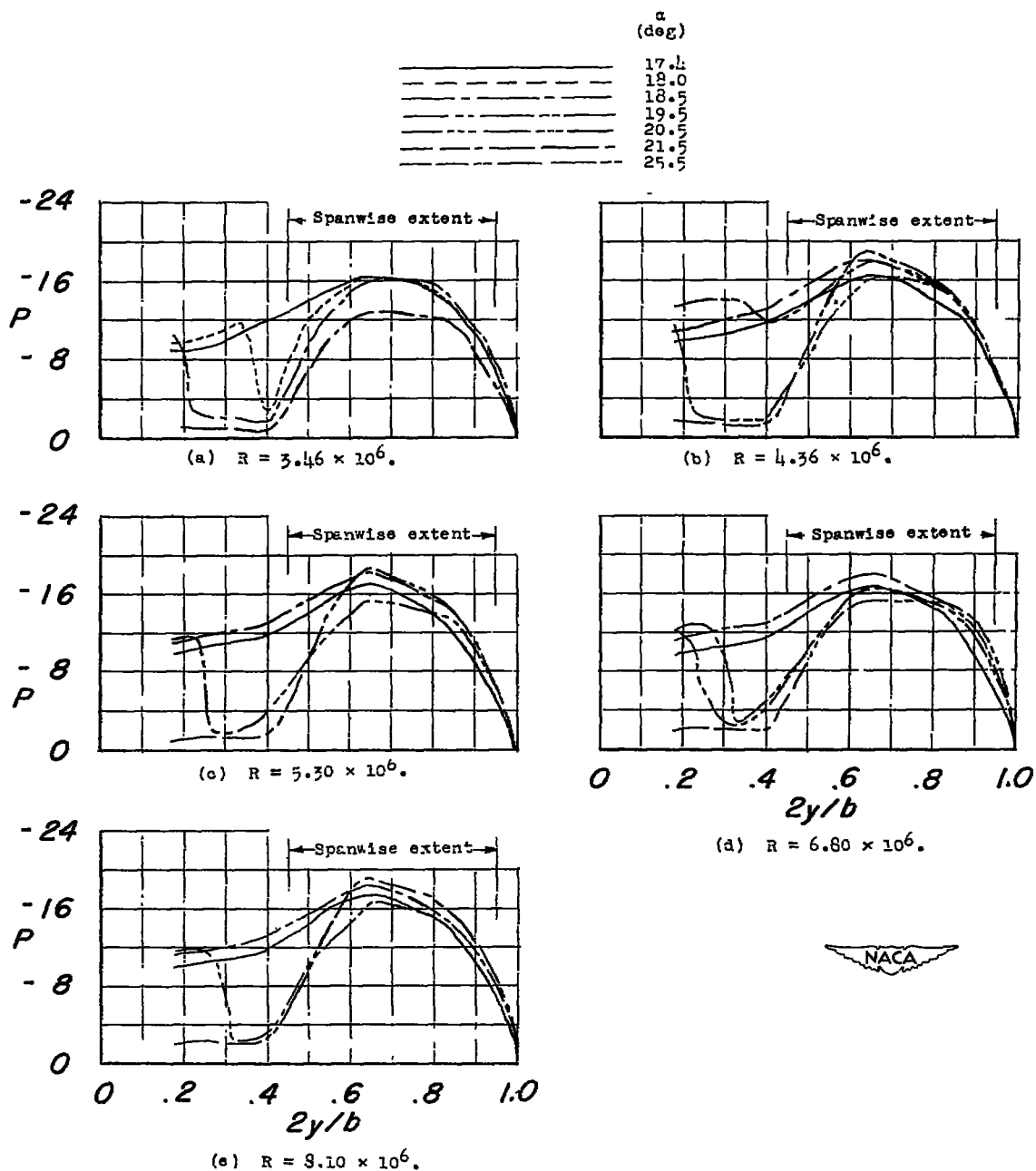


Figure 20.- Effects of Reynolds number variation on the leading-edge pressure coefficients of the 37° sweptback wing. Porosity A; spanwise extent, $0.45b/2$ to $0.95b/2$; chordwise extent, 0 to $0.015c$; $C_Q = 0.00040$.

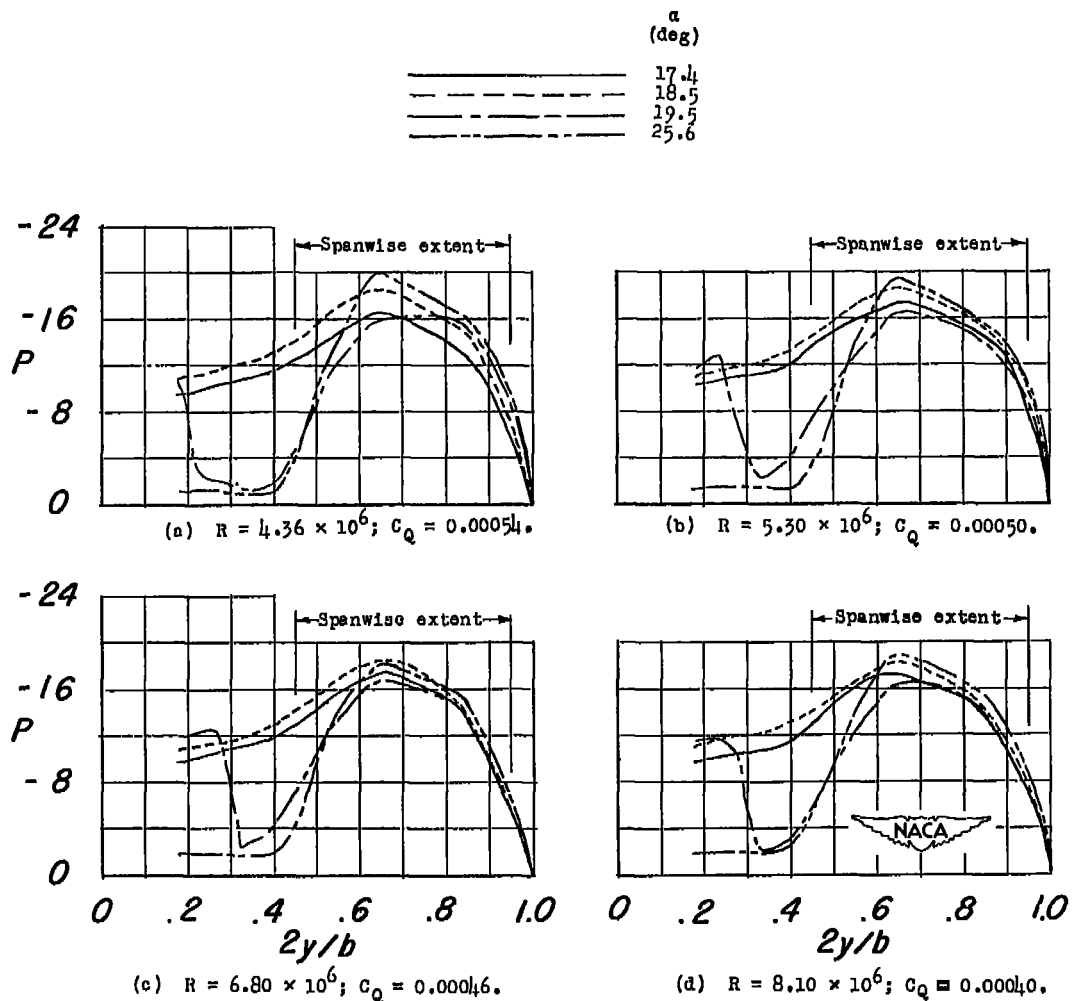
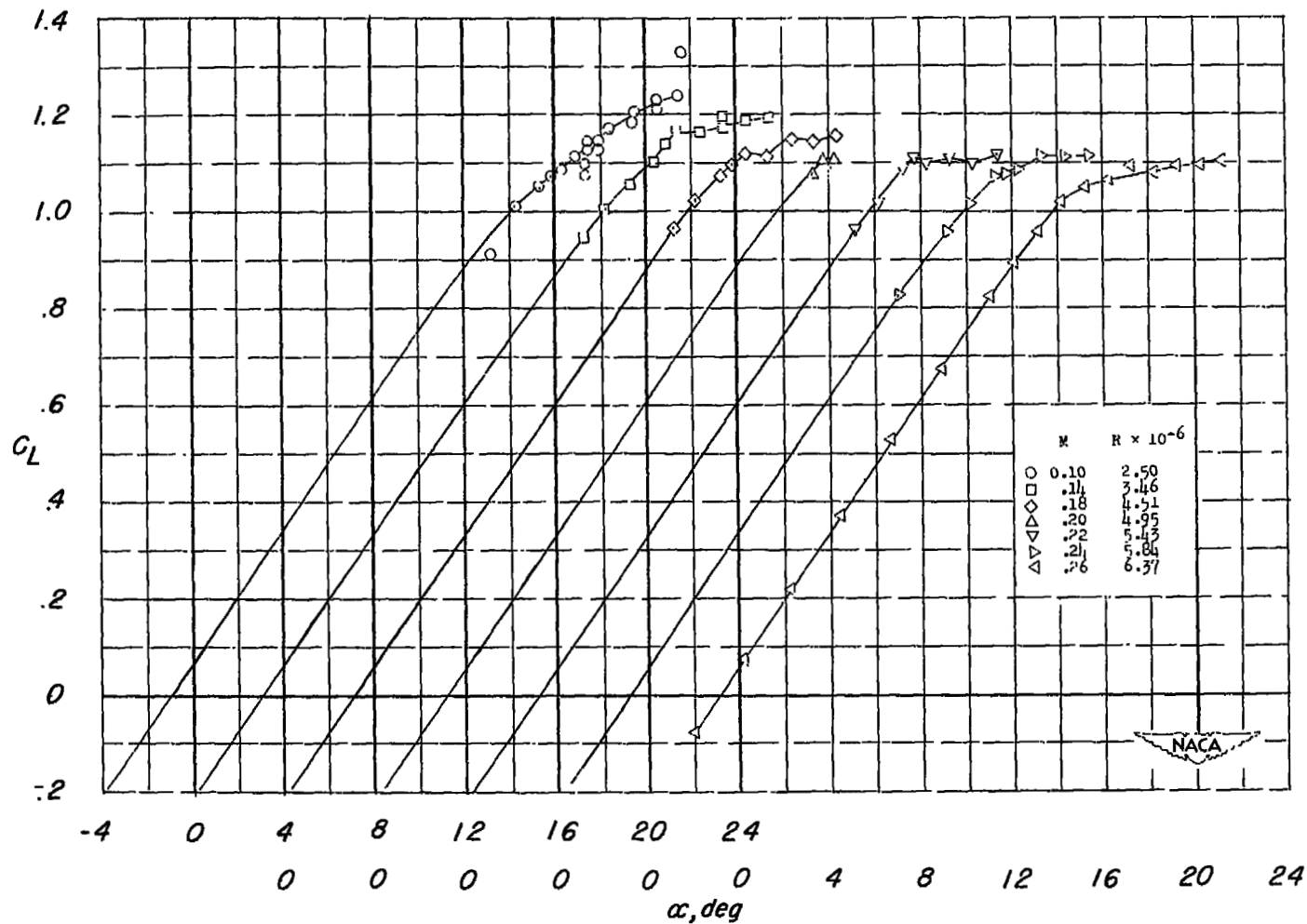
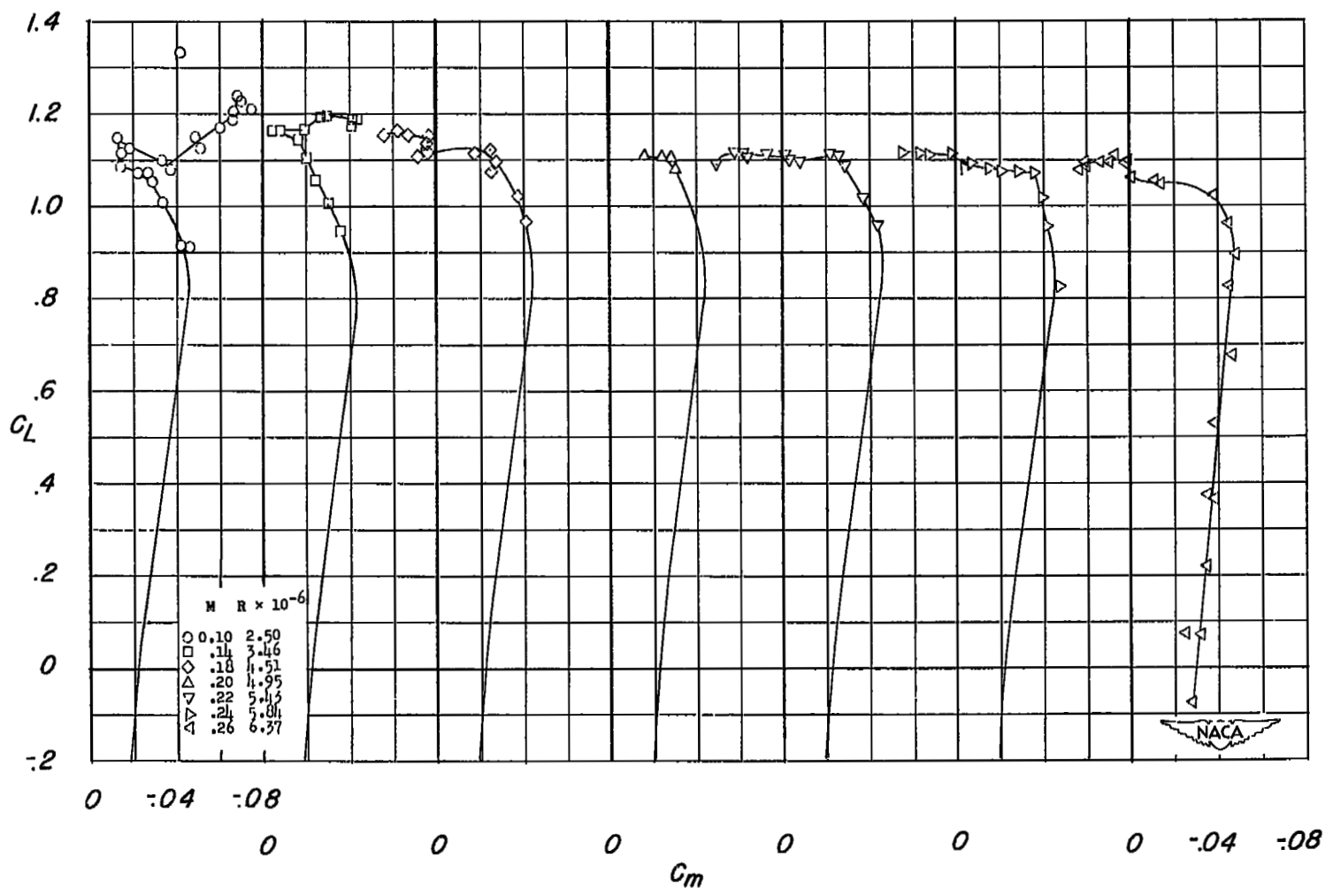


Figure 21.- Effects of Reynolds number variation on the leading-edge pressure coefficients of the 37° sweptback wing. Porosity A; spanwise extent, $0.45b/2$ to $0.95b/2$; chordwise extent, 0 to $0.015c$; $C_Q R^{1/2} \approx 0.00040 \sqrt{8.10 \times 10^6}$.



(a) C_L against α .

Figure 22.- Effects of Mach number and Reynolds number variation on the aerodynamic characteristics of the 37° sweptback wing. Porosity A; spanwise extent, $0.45b/2$ to $0.95b/2$; chordwise extent, 0 to $0.015c$; $C_Q \approx 0.00015$.



(b) C_L against C_m .

Figure 22.- Concluded.

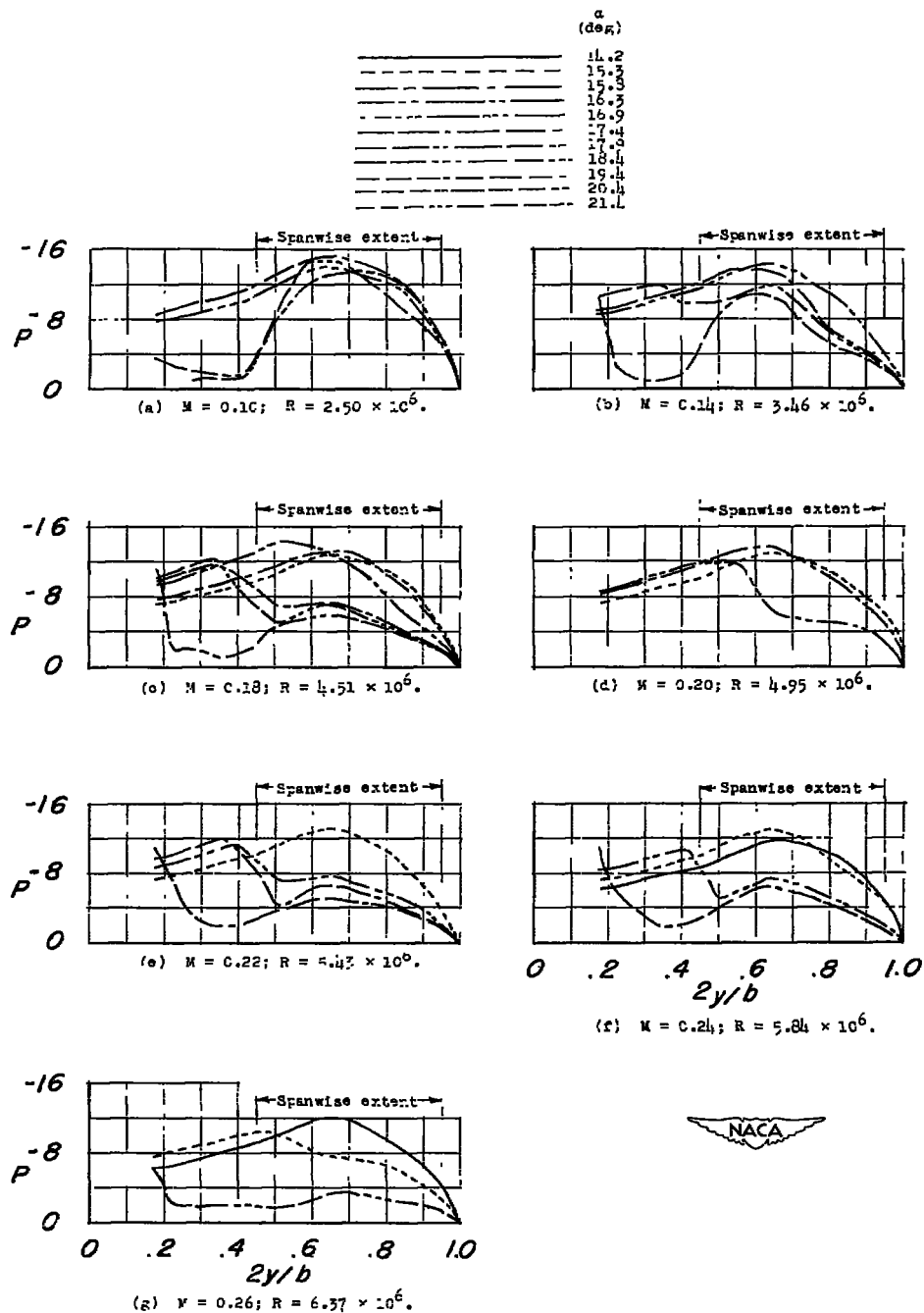


Figure 23.- Effects of Mach number and Reynolds number variation on the leading-edge pressure coefficients of the 37° sweptback wing. Porosity A; spanwise extent, $0.45b/2$ to $0.95b/2$; chordwise extent, 0 to $0.015c$; $C_Q \approx 0.00015$.

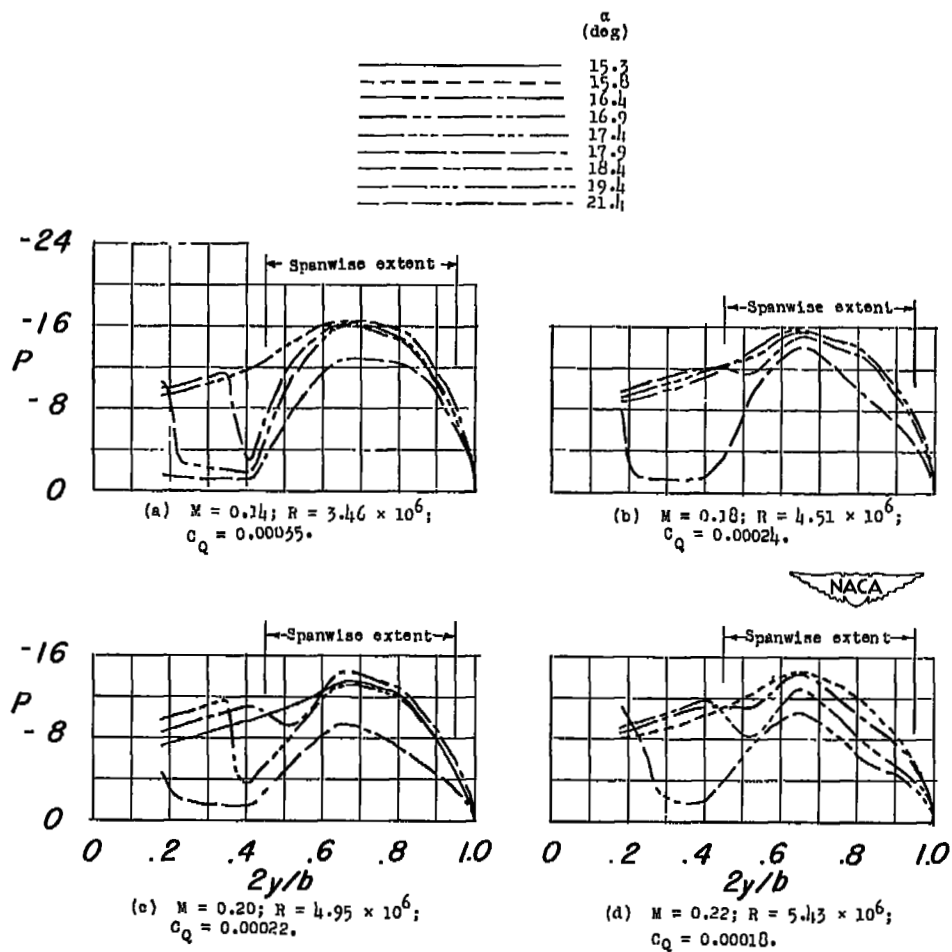


Figure 24.- Effects of Mach number and Reynolds number variation on the leading-edge pressure coefficients of the 37° sweptback wing. Porosity A; spanwise extent, $0.45b/2$ to $0.95b/2$; chordwise extent, 0 to $0.015c$; $C_Q =$ maximum available.

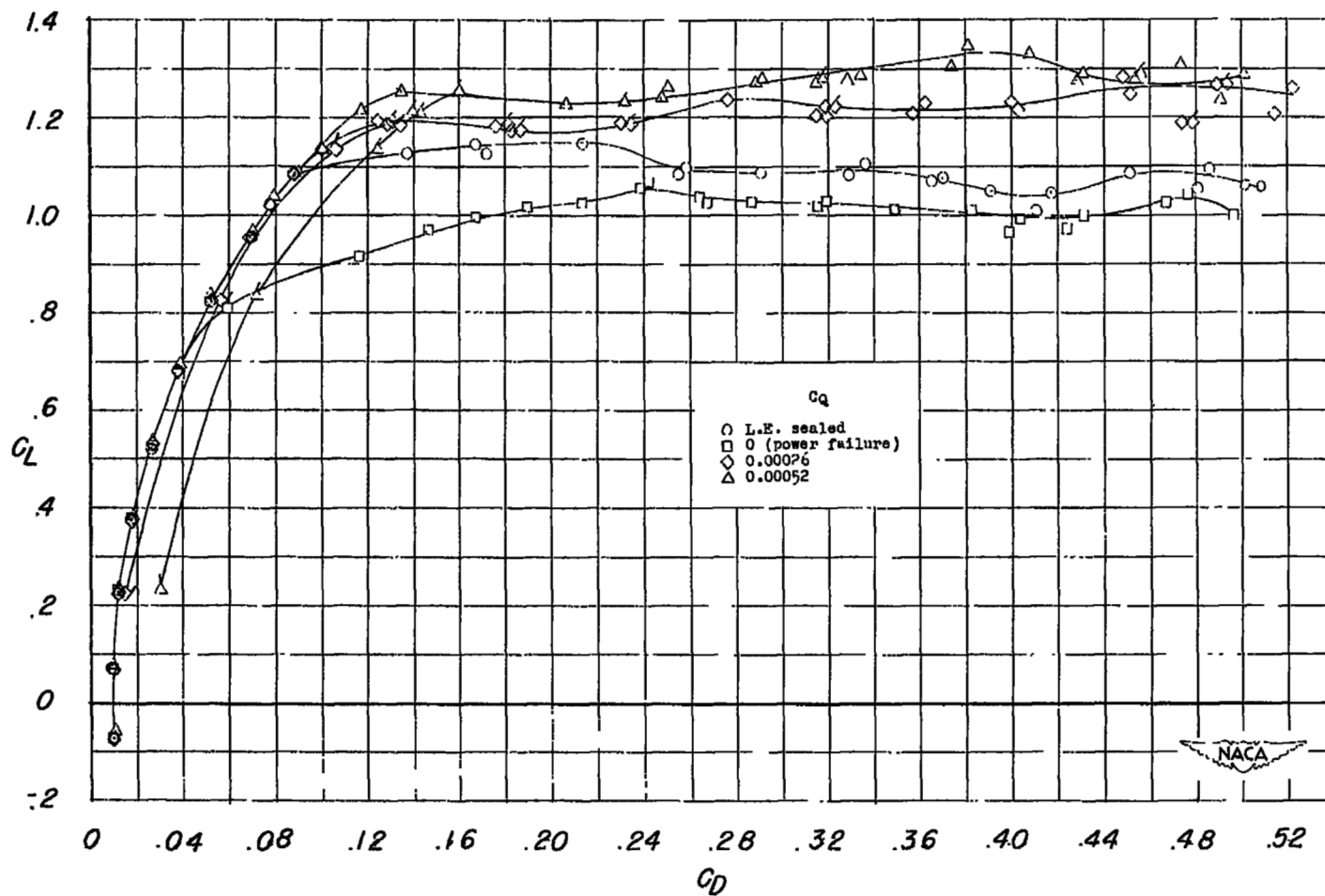


Figure 25.- Effects of leading-edge suction on the drag characteristics of the 37° sweptback wing. Porosity A; spanwise extent, $0.45b/2$ to $0.95b/2$; chordwise extent, 0 to $0.015c$; $R = 6.80 \times 10^6$; $M = 0.12$; flagged symbol drag includes C_{Dp} .

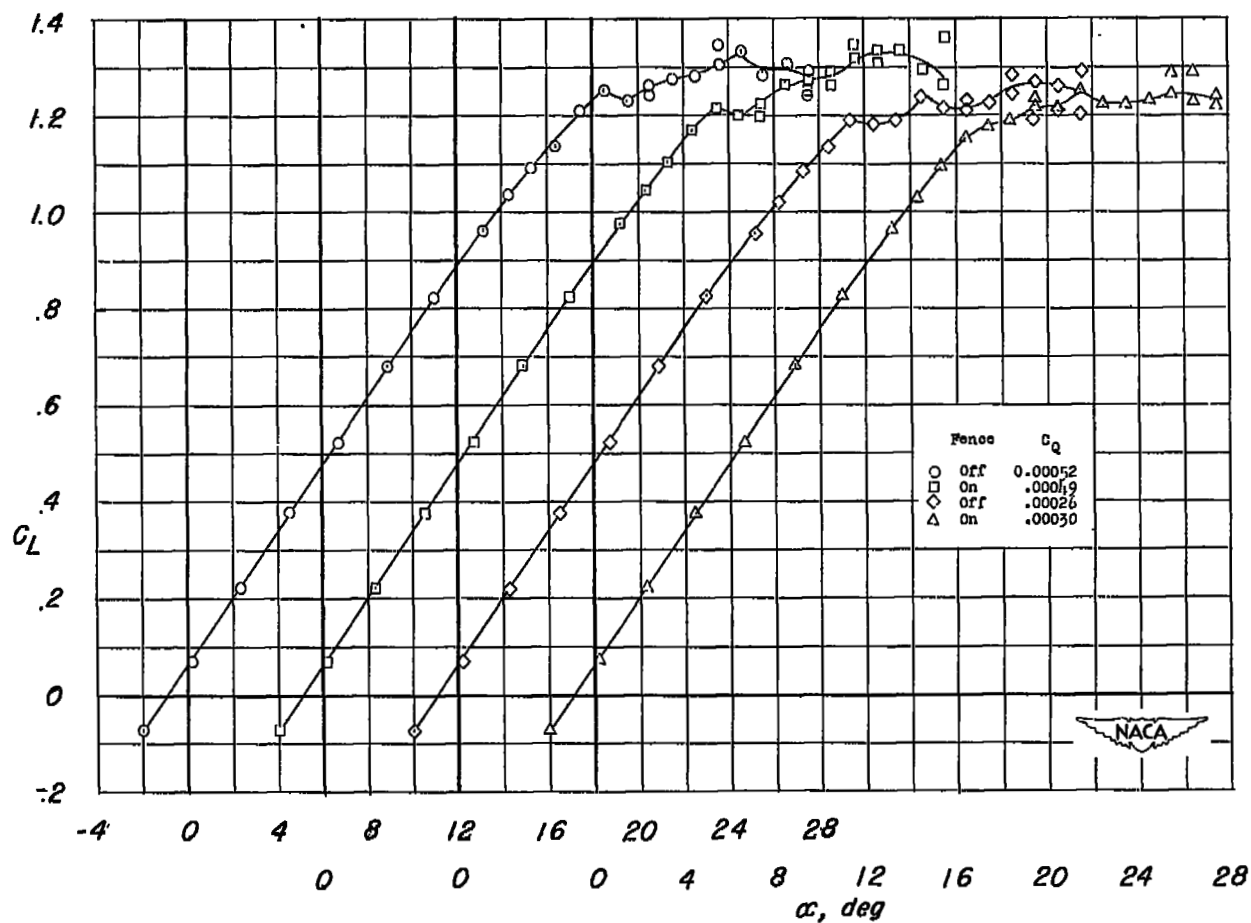
(a) C_L against α .

Figure 26.- Effects of an upper-surface fence on the aerodynamic characteristics of the 37° sweptback wing. Porosity A; spanwise extent, $0.45b/2$ to $0.95b/2$; chordwise extent, 0 to $0.015c$; $R = 6.80 \times 10^6$; $M = 0.12$.

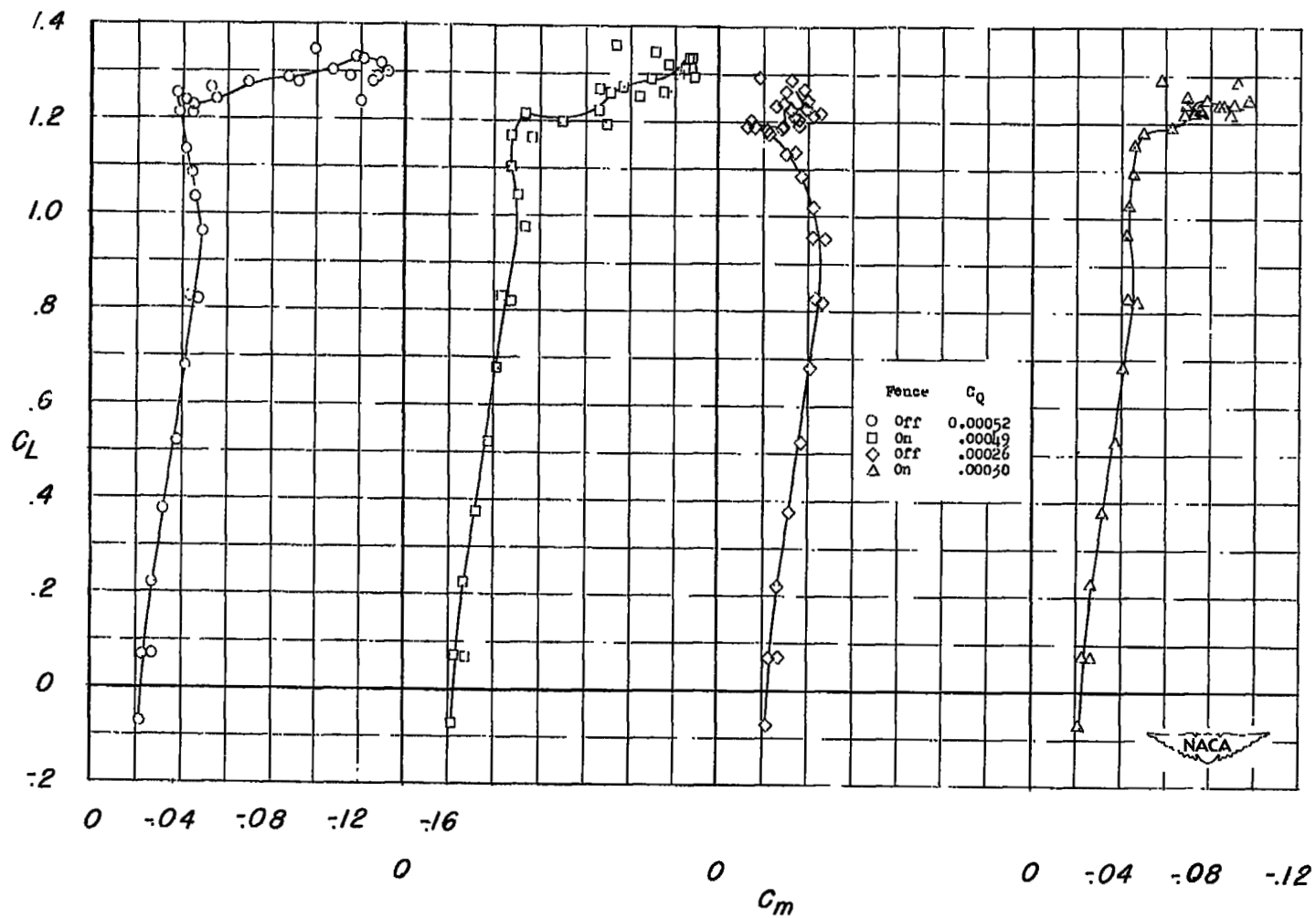
(b) C_L against C_m .

Figure 26.- Concluded.

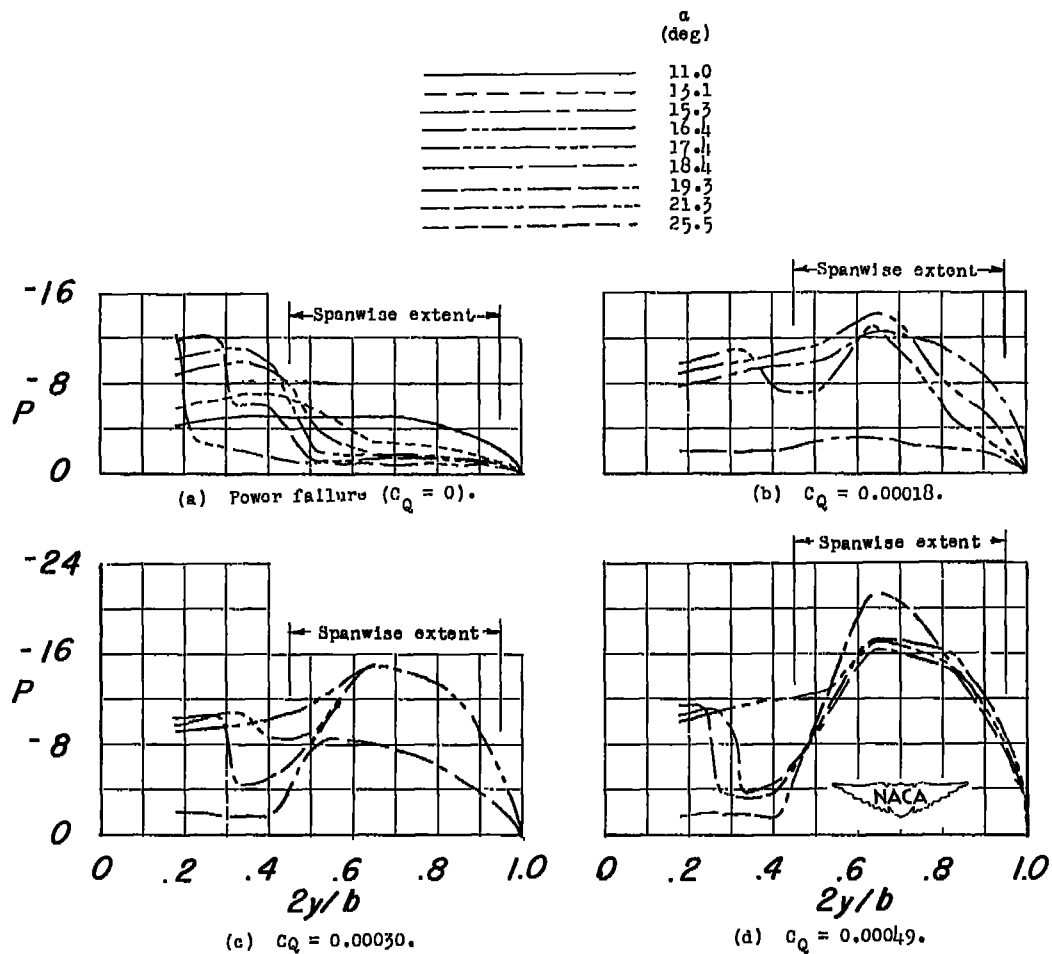


Figure 27.- Effects of an upper-surface fence on the leading-edge pressure coefficients of the 37° sweptback wing. Porosity A; spanwise extent, $0.45b/2$ to $0.95b/2$; chordwise extent, 0 to $0.015c$; $R = 6.80 \times 10^6$; $M = 0.12$.

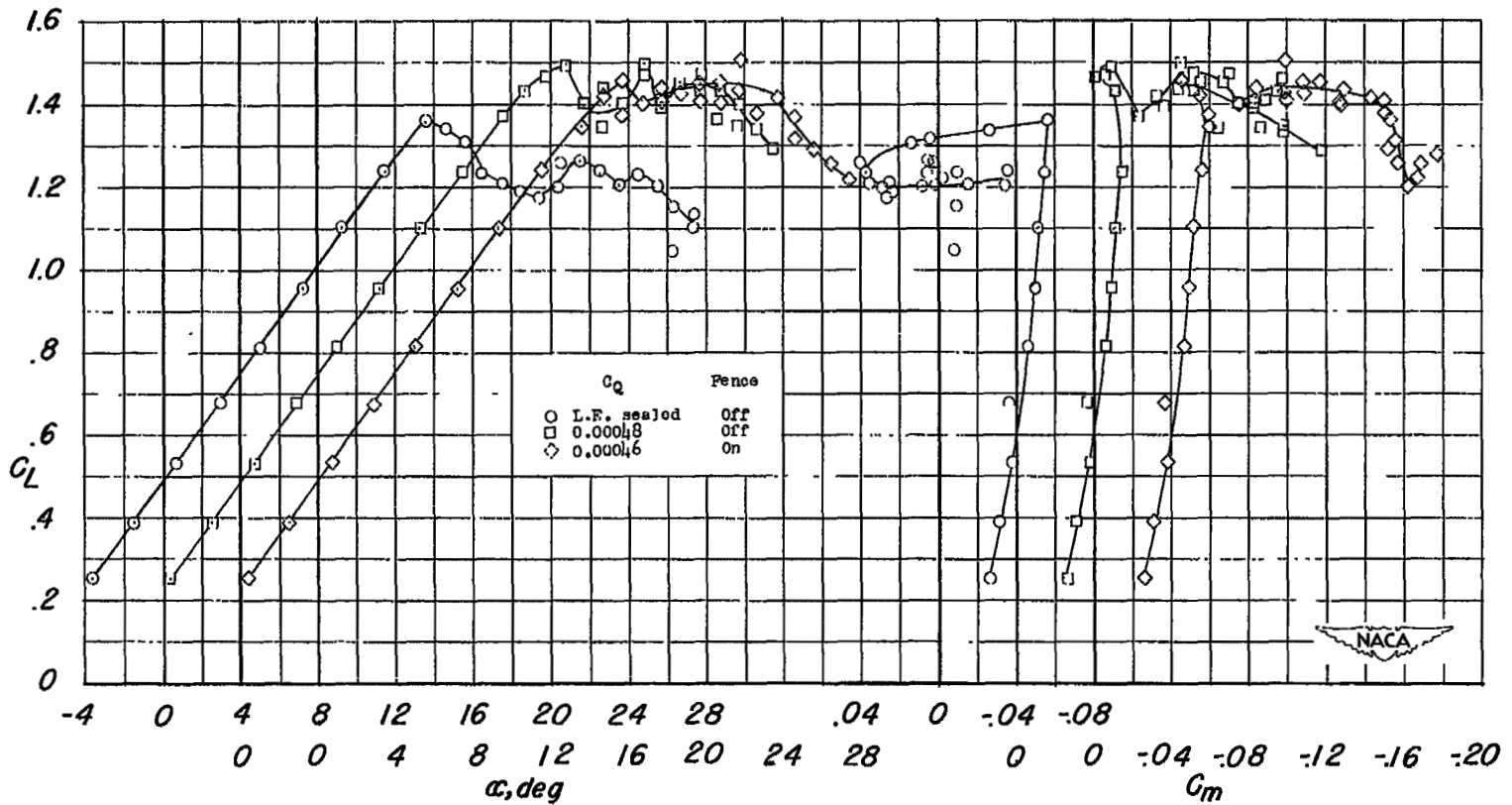


Figure 28.- Effects of leading-edge suction and an upper-surface fence on the aerodynamic characteristics of the 37° sweptback wing with half-span split flap. Porosity A; spanwise extent, $0.45b/2$ to $0.95b/2$; chordwise extent, 0 to $0.015c$; $R = 6.80 \times 10^6$; $M = 0.12$.

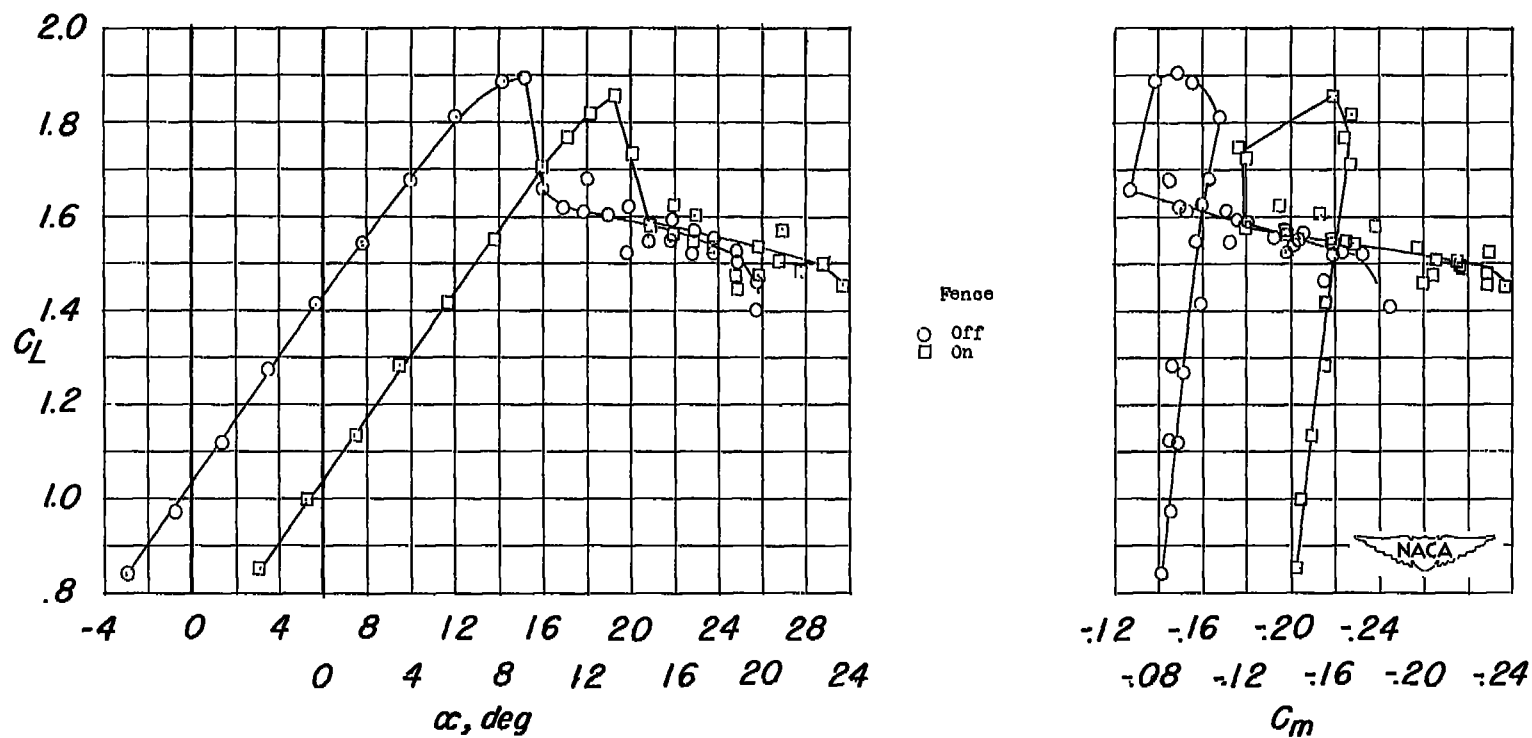


Figure 29.- Effects of an upper-surface fence on the aerodynamic characteristics of the 37° sweptback wing with half-span double slotted flap. Porosity A; spanwise extent, $0.45b/2$ to $0.95b/2$; chordwise extent, 0 to $0.015c$; $C_Q = 0.00048$; $R = 6.80 \times 10^6$; $M = 0.12$.

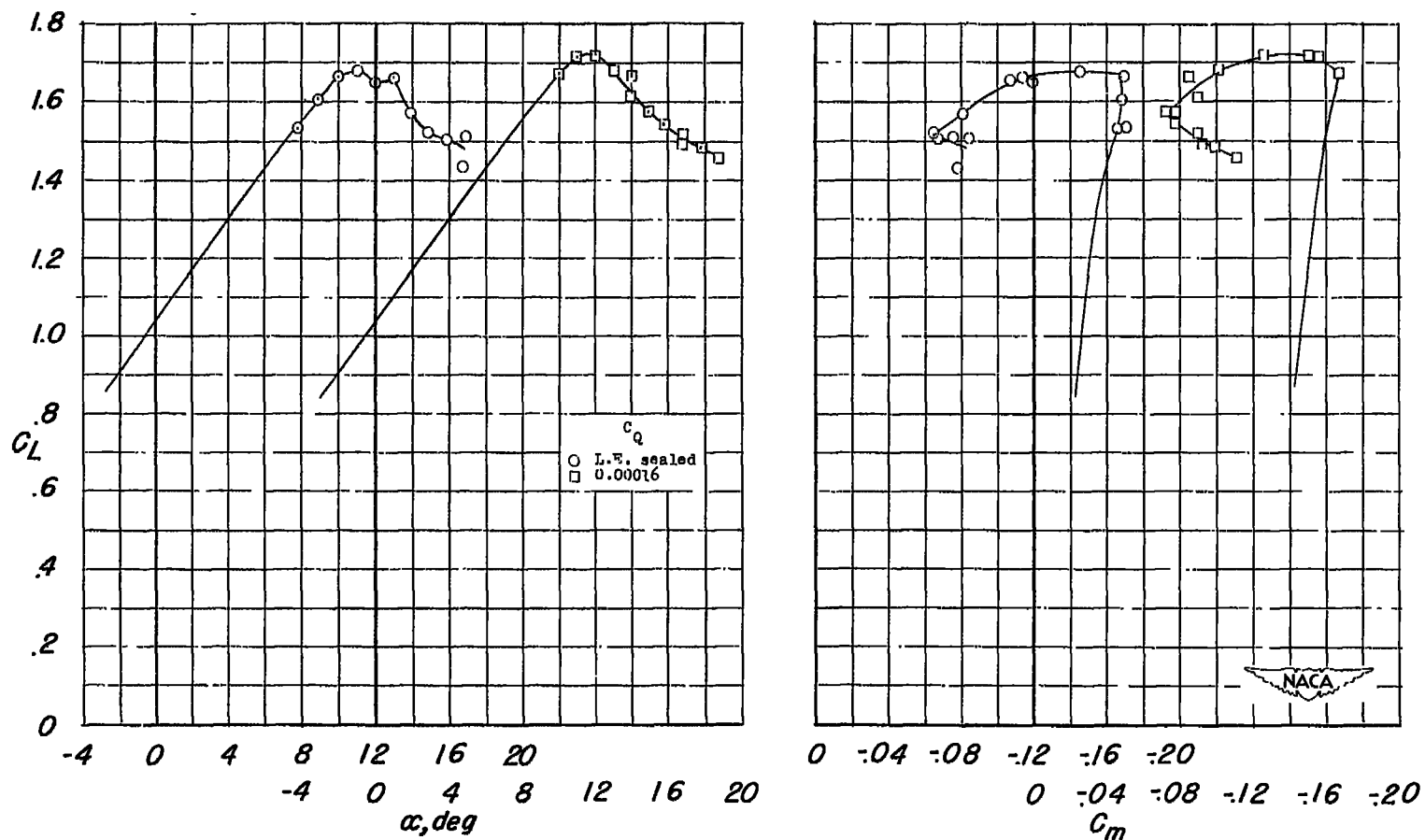


Figure 30.- Effects of leading-edge suction on the aerodynamic characteristics of the 37° sweptback wing with half-span double slotted flap. Porosity A; spanwise extent, $0.45b/2$ to $0.95b/2$; chordwise extent, 0 to $0.015c$; $R = 5.84 \times 10^6$; $M = 0.24$.

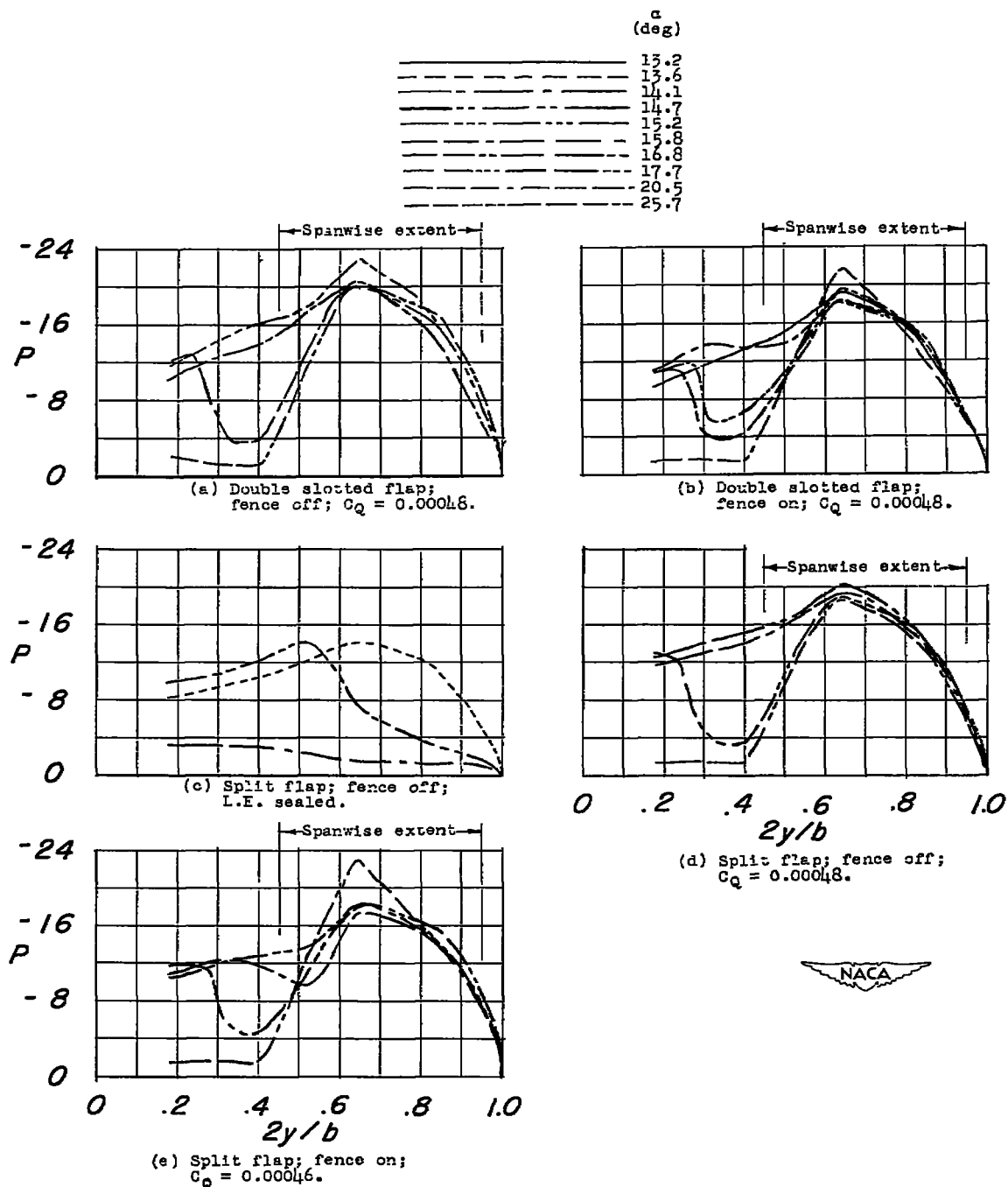


Figure 31.- Effects of leading-edge suction and an upper-surface fence on the leading-edge pressure coefficients of the 37° sweptback wing with half-span flap. Porosity A; spanwise extent, $0.45b/2$ to $0.95b/2$; chordwise extent, 0 to $0.015c$; $R = 6.80 \times 10^6$; $M = 0.12$.

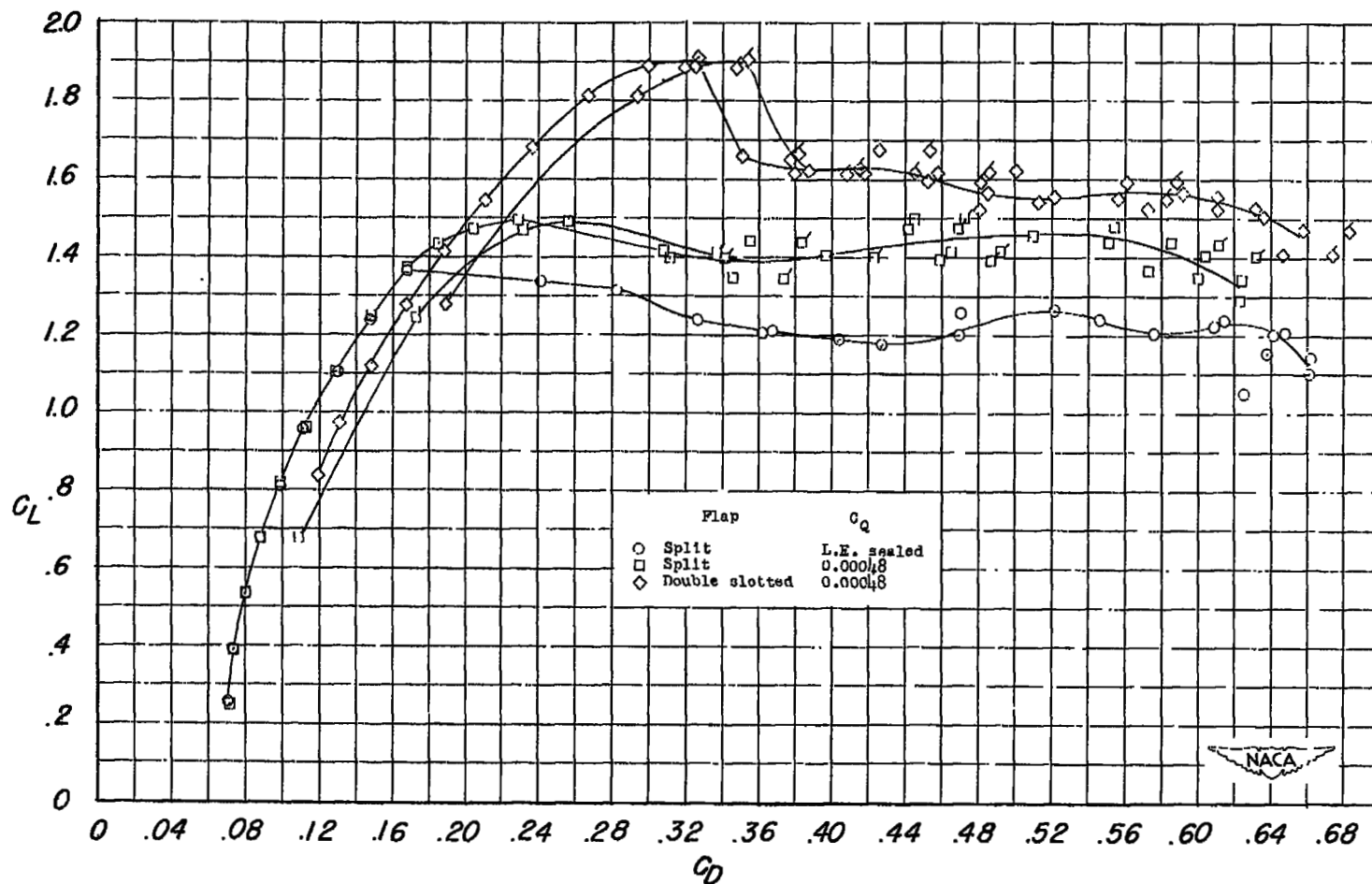


Figure 32.- Effects of leading-edge suction on the drag characteristics of the 37° sweptback wing with half-span flaps. Porosity A; spanwise extent, $0.45b/2$ to $0.95b/2$; chordwise extent, 0 to $0.015c$; $R = 6.80 \times 10^6$; $M = 0.12$; flagged-symbol drag includes C_{Dp} .

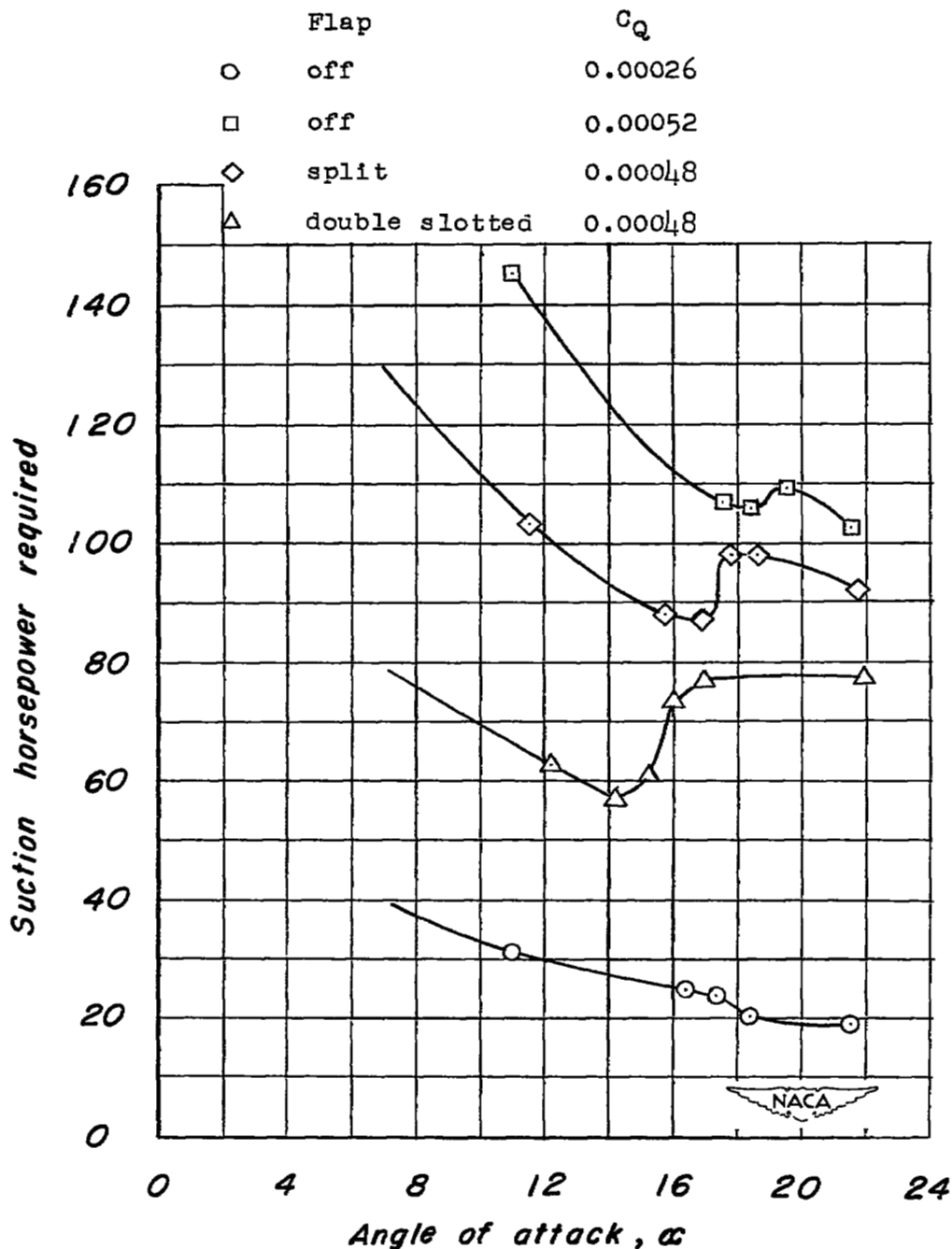


Figure 33.- Variation of calculated suction horsepower with angle of attack of a hypothetical airplane with 37° sweptback wing. Assumed wing loading, 50 pounds per square foot; assumed wing area, 306.1 square feet; porosity A; spanwise extent, $0.45b/2$ to $0.95b/2$; chordwise extent, 0 to $0.015c$.